Characterization of a cysteine protease from *Phytolacca americana* and its association with Pokeweed Antiviral Protein

Annabelle Audet

A thesis submitted to the Faculty of Graduate Studies
in partial fulfilment of the requirements for the degree of

MASTER OF SCIENCE

Graduate Program in Biology
York University
Toronto, Ontario

August 2024

ABSTRACT

The plant apoplast, an essential extracellular space, contains diverse proteins crucial for plant defence. This study focuses on *Phytolacca americana* (American pokeweed), examining the interaction between the ribosome inactivating protein Pokeweed Antiviral Protein (PAP) and a putative papain-like cysteine protease, *Phytolacca americana* cysteine protease 1 (PaCP1). Bioinformatic predictions identified PaCP1 as a papain-like cysteine protease with conserved structural features, while enzymatic assays confirmed its functionality. Yeast-two hybrid assays validated the interaction between PAP and PaCP1, and localization studies indicated their extracellular co-localization in the apoplast. Enzymatic assays further demonstrated PaCP1's ability to cleave PAP, with mass spectrometry identifying the resulting degradation products. Differential expression studies under salicylic acid and Flg22 treatment revealed different patterns of expression for both PAP and PaCP1. This research enhances our understanding of PAP and its protein interactions as well as its potential role in the pokeweed apoplast.

ACKNOLEDGMENTS

First and foremost, I am deeply grateful to my supervisor, Dr. Kathi Hudak, for providing me with the incredible opportunity to undertake this project in her lab. It has been an amazing journey to work under your supervision, contributing to and learning from your bright ideas. Your patience, insight, and unwavering support have been instrumental during this part of my graduate studies. Your enthusiasm for research, attention to detail, and confidence in your students have significantly fostered my development as a scientist. Thank you for helping me turn our lab office into a miniature botanical garden.

I am also grateful to my committee member, Dr. Nik Kovinich, for your time, constructive comments, and advice. I would also like to thank Dr. Peter Cheung and Dr. Rolando Ceddia for agreeing to be on my examination committee and taking the time to read my thesis.

A heartfelt thank you to my lab colleague and friend, Tanya Prashar, for your camaraderie, support, and discussions that have helped me grow as a researcher. Your help in the lab and encouragement during challenging times were crucial to the success of this project.

Special thanks to my family for their love, patience, and belief in me. One day you might be able to understand truly what it is that I am working on.

I would like to thank my best friend for your love and patience. You have been by my side, offering support, encouragement, and picking me up at ridiculous hours of the night. Your presence has been a source of strength and has not gone unnoticed.

Finally, I would also like to extend my gratitude to my past self for not giving up, even during the most challenging times. Thank you for persevering, for believing in your potential, and for pushing through every obstacle. Thank you for waking up every day and putting up with the lengthy commute even when sleeping in sounds like a better option. Your dedication and hard work have made this achievement possible.

To everyone who contributed to this thesis, directly or indirectly, I am truly grateful. This achievement would not have been possible without your support.

Thank you :)

TABLE OF CONTENTS

LIST OF TABLES

LIST OF FIGURES

LIST OF COMMON ABBREVIATIONS

AF	Apoplastic Fluid
AtXCP1	*Arabidopsis thaliana* Xylem Cysteine Protease 1
DAMPs	Damage-Associated Molecular Patterns
dH$_2$O	Distilled water
eGFP	Enhanced Green Fluorescence Protein
ER	Endoplasmic Reticulum
EV	Empty Vector
His	Histidine
JA	Jasmonic Acid
kDa	Kilodaltons
Leu	Leucine
MAMPs	Microbe-Associated Molecular Patterns
MAPK	Mitogen-Activated Protein Kinase
miRNAs	microRNAs
PaCP1	*Phytolacca americana* Cysteine Protease 1
PAP	Pokeweed Antiviral Protein
PAPx	Inactive mutant of PAP
PCD	Programmed cell death
PLCP	Papain-Like Cysteine Protease
PR	Pathogenesis Related
PRR	Pathogen Recognition Receptors
qPCR	Quantitative PCR
RFU	Relative Fluorescence Units
RIP	Ribosome Inactivating Protein
ROS	Reactive Oxygen Species
rRNA	Ribosomal RNA
RT	Reverse Transcription
RT-PCR	Reverse Transcription Polymerase Chain Reaction
SA	Salicylic Acid
SAR	Systemic Acquired Resistance
siRNAs	small interfering RNAs
SRL	Sarcin-Ricin Loop
sRNAs	small RNAs
TFs	Transcription Factors
Trp	Tryptophan

1. INTRODUCTION

1.1 The Apoplast

1.1.1 General characteristics

The plant apoplast, an integral component of a plant's physiology, plays a crucial role in various biological processes, including nutrient transport, signalling, and defence against pathogens. It encompasses the cell walls, intercellular space, and the xylem, extending from the plant's outer surface to the internal tissues (Figure 1; Farvardin et al., 2020). The apoplast serves as both a physical barrier and a dynamic site for the plant's immune responses, making it a frontline defence against pathogenic attacks. This complex matrix is the first barrier between plant cells and their environment, mediating numerous interactions that are vital for plant adaptation and survival (Darino et al., 2022).

The cell walls, which are primarily composed of polysaccharides such as cellulose, hemicellulose, and pectin, provide mechanical support and protection against environmental stresses (Cosgrove, 2015). Intercellular spaces, filled with aqueous solutions, facilitate the movement of water, nutrients, and signalling molecules between cells (Cosgrove, 2018). The xylem vessels function in the long-distance transport of water, minerals and organic compounds throughout the plant (Taiz et al., 2015). Water and mineral nutrients are transported through the apoplast via the transpiration stream, facilitated by the cohesive and adhesive properties of water and the presence of ion channels and transporters (Taiz et al., 2015).

The apoplast exhibits a diverse biochemical composition, comprising sugars, amino acids, enzymes, hormones, secondary metabolites, and stress-related proteins essential for various physiological processes (Darino et al., 2022). Its content varies significantly depending on the plant's physiological state, environmental conditions, organ and tissue type, underscoring its dynamic nature and fundamental role in plant response to abiotic and biotic stresses (Farvardin et al., 2020). In response to environmental stresses such as drought, salinity, and pathogen attacks, the apoplast undergoes dynamic changes, including alterations in cell wall composition, activation of defence related enzymes, and accumulation of antimicrobial compounds (Miedes et al., 2014). The apoplast serves as a signalling hub, mediating communication between cells and tissues and coordinating responses to internal and external cues (Darino et al., 2022). Proteomic analyses have

identified a wide array of proteins in the apoplast, including cell wall remodelling, defence proteins, and signalling molecules (Delaunois et al., 2013; Delaunois et al., 2014; Gupta et al., 2015; Jiang et al., 2023). The diversity of proteins present in the apoplast underscores its versatile roles in plant physiology and defence, supporting fundamental processes like growth and nutrient transport while equipping plants with the tools needed to sense and respond to environmental challenges.

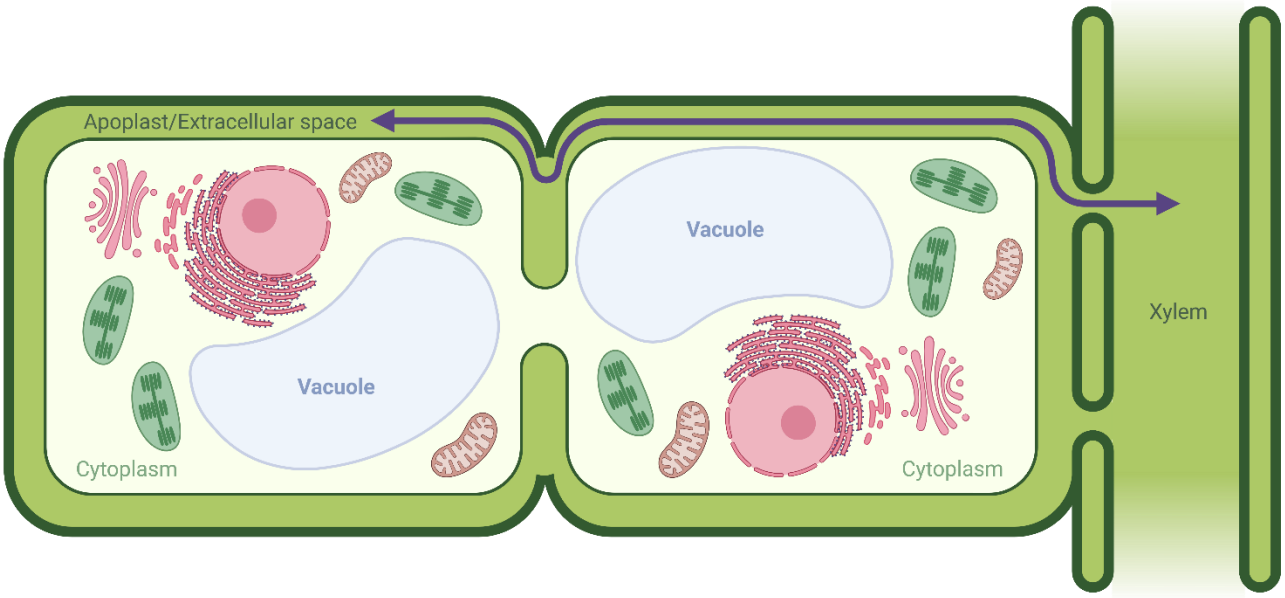

Figure 1. Schematic of the apoplastic/extracellular space in plant cells as distinct from cytoplasm. The purple arrow indicates the connection between the apoplast and the xylem. Created with BioRender.com

1.1.2 Apoplast during environmental stresses

In the context of plant-pathogen interactions, the apoplast is a primary battleground where initial contact and early stages of infection occur. Pathogens, such as bacteria, fungi, and oomycetes, must navigate and exploit the apoplast as a route of entry into plant tissues, secreting virulence factors to overcome plant defences (Mott et al., 2014). In response, plants deploy an array of defence strategies, including the secretion of antimicrobial compounds, reinforcement of the cell wall, and activation of defence-related signalling pathways that trigger broader immune responses (Darino et al., 2022)

One of the earliest responses is the production of reactive oxygen species (ROS), which have direct deleterious effects on pathogens and lead to the strengthening of the cell wall to prevent

pathogen penetration (Wang et al., 2020; Farvardin et al., 2020). ROS are natural products generated by various metabolic reactions in cells. They serve as secondary messengers in different physiological processes and play a dual role in plant biology (Mott et al., 2014). While ROS are crucial for signalling pathways that control plant growth and response to stresses, their overaccumulation can lead to oxidative damage and programmed cell death (PCD) (Farvardin et al., 2020). The balance between ROS production and scavenging is therefore vital for maintaining cellular homeostasis and effective immune response.

Nutrient availability in the apoplast also plays a critical role in plant defence. Pathogens often manipulate the apoplastic sugar content to facilitate their own growth and proliferation. For example, bacteria can induce the expression of plant sugar transporters like SWEET11, which releases sugars into the apoplast, providing a nutrient rich environment for the pathogens (Chen et al., 2010). In response, plants can alter the expression of other sugar transporters to reduce free sugar levels in the apoplast, thereby restricting pathogen access to these nutrients (Chen et al., 2010).

Moreover, the pH of the apoplast is a dynamic attribute that plays a vital role in various physiological processes, including nutrient uptake, enzyme activity, and defence responses. The apoplastic pH typically ranges from 4.5 to 5.5, but it can fluctuate in response to environmental conditions and stress factors (Geilfus et al., 2020a). It has been demonstrated in several cases that a variety of abiotic and biotic stresses can induce alkalinization of the apoplast (Felle, 2001; Felle et al., 2004; Felle et al., 2009; Geilfus, 2017). Since measuring apoplastic pH in real-time without disrupting the plant is challenging, many aspects of its dynamics remain unclear, making it a continued focus of research. However, it has been suggested that changes in the apoplastic pH during pathogen infection can influence the availability of various defence molecules and nutrients (Geilfus et al., 2020b).

Recent studies have highlighted the importance of small RNAs (sRNA) in apoplastic defence. These include microRNAs (miRNAs) and small interfering RNAs (siRNAs), which regulate various cellular processes, including immune responses during plant-pathogen interactions via RNA interference (RNAi) pathways (Karimi et al., 2022). sRNAs are often found outside extracellular vesicles (EVs) in the apoplast, protected by RNA-binding proteins, which prevent their degradation by nucleases (Karimi et al., 2022). Additionally, long non-coding RNAs

(lncRNAs) are secreted into the apoplast, and their function still remains unknown, however the authors suggest they may play a role in sequestering pathogen-derived sRNA effectors, thus enhancing host immunity (Karimi et al., 2022).

Pathogen recognition in the apoplast involves the detection of microbe-associated molecular patterns (MAMPs) by pattern recognition receptors (PRRs) located on the plant cell surface (Jones & Dangl, 2006; Zhou & Zhang, 2020). This interaction triggers the secretion of pathogenesis-related (PR) proteins and other defence related proteins into the apoplast. Proteases, such as papain-like cysteine proteases (PLCPs), are particularly important in apoplastic immunity. Their activity produces small peptides that act as damage-associated molecular patterns (DAMPs), further activating the plant's immune response (Ziemann et al., 2018; Chen et al., 2023).

1.2 Proteases

1.2.1 General overview of proteases

Proteases, also known as peptidases or proteinases, are enzymes that catalyse the hydrolysis of peptide bonds in proteins, leading to their degradation into smaller polypeptides or amino acids (Godson & van der Hoorn, 2021). They play essential roles in all forms of life through various biological processes, including protein turnover, signal transduction, apoptosis, and the immune response (van der Hoorn, 2008). In plants, proteases are involved in development, stress responses, and defence mechanisms. They regulate processes such as seed germination, senescence, and programmed cell death (PCD), which are crucial for plant growth and survival (Godson & van der Hoorn, 2021). The MEROPS database classifies plant proteases into five families based on their catalytic mechanisms: aspartic, cysteine, metalloproteases, threonine, and serine (Rawlings & Bateman, 2020). Each class of proteases has unique characteristics and functions that contribute to the overall proteolytic activity within the plant system. The activity of proteases must be tightly regulated to ensure proper cellular function and to prevent unintended proteolysis that could be detrimental to cells (van der Hoorn, 2008).

1.2.2 Apoplastic proteases

Apoplastic proteases are those located within the extracellular space and are critical for plant-environment interactions. These proteases play a vital role in maintaining cellular homeostasis and mediating plant responses to various environmental challenges by participating in cell wall remodelling, signalling, and defence mechanisms against pathogens (Jashni et al.,

2015; Godson & van der Hoorn, 2021; Wang et al., 2020). Apoplastic proteases are particularly important in the context of plant immunity, where they modulate the plant's defence responses through the processing of immune-related proteins and peptides (Godson & van der Hoorn, 2021; Wang et al., 2020).

1.2.3 Cysteine proteases in the apoplast

Among the various classes of apoplastic proteases, cysteine proteases play significant roles in plant physiology and defence. Cysteine proteases utilise a cysteine residue in their active site to catalyse the cleavage of peptide bonds (Misas-Villamil et al., 2016). They are involved in processes such as PCD, senescence, and defence against pathogens (Misas-Villamil et al., 2016). The activity and function of these proteases are tightly regulated to prevent unwarranted proteolysis that could be detrimental to the plant cells (van der Hoorn, 2008). Papain-like cysteine proteases (PLCPs) constitute a prominent subclass of cysteine proteases. They are named after papain, a well-studied protease from the papaya plant, and are characterised by their conserved cysteine-histidine-asparagine catalytic triad (Figure 2; Misas-Villamil et al., 2016). PLCPs are implicated in a variety of plant functions, including protein turnover, maturation of defence proteins, and regulation of signalling pathways (Liu et al., 2018; Misas-Villamil et al., 2016). These proteases are also central to the plant's immune response, where they participate in the degradation of pathogen-derived proteins and the activation of immune signalling (Misas-Villamil et al., 2016; Shindo & van der Hoorn, 2007).

The regulation of PLCP activity is crucial for maintaining cellular homeostasis and effective immune responses. PLCPs are regulated at multiple levels, including transcriptional control, post-translational modifications, and interaction with inhibitors (Misas-Villamil et al., 2016). For example, the expression of certain PLCPs is upregulated in response to pathogen infection, while cysteine protease inhibitors, such as cystatins, can directly inhibit PLCP activity to prevent excessive proteolysis (Pérez-López et al., 2021). Moreover, PLCPs are often compartmentalised within specific subcellular locations, including the apoplast and vacuole, where their activity can be precisely controlled in response to external stimuli. This spatial regulation allows plants to deploy PLCPs effectively during pathogen attack, ensuring a rapid and targeted immune response (Wang et al., 2020).

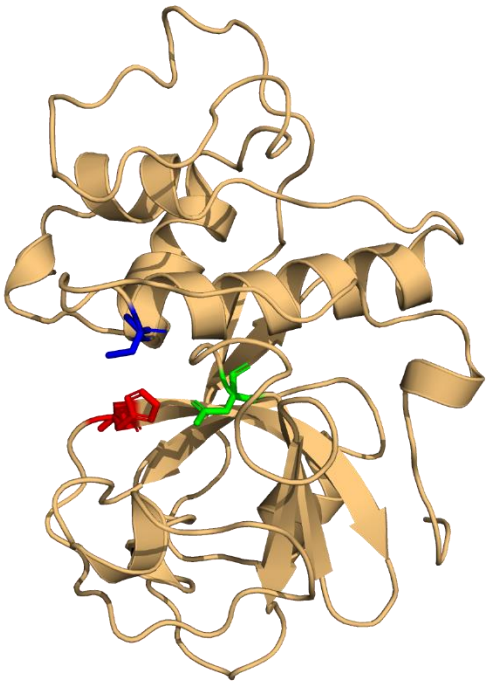

Figure 2. Cartoon representation of the 3D structure of papain. The 3D structure of papain was obtained from the AlphaFold Protein Structure Database (Jumper et al., 2021; Váradi et al., 2023). The structure of the active form of papain is coloured in orange. The residues of the active site are coloured in blue, red and green and represent cysteine (C158), histidine (H292), asparagine (N308), respectively.

1.2.4 Role of PLCPs in plant immunity

PLCPs are involved in the activation and regulation of plant immune responses. They process and activate pathogenesis-related (PR) proteins and other defence molecules that are secreted into the apoplast during pathogen attack. For example, PLCPs such as *Arabidopsis thaliana* xylem cysteine protease 1 (XCP1) cleave pathogenesis-related (PR) proteins into smaller peptides that enhance the plant's immune response (Chen et al., 2023). Additionally, PLCPs can generate damage-associated molecular patterns (DAMPs) by degrading endogenous substrates, which then act as signals to trigger further immune responses (Misas-Villamil et al., 2016).

1.3 Elicitors of plant immune response

1.3.1 Salicylic acid (SA) and jasmonic acid (JA)

Salicylic acid (SA) and jasmonic acid (JA) are critical phytohormones involved in the regulation of plant immune responses. SA, in particular, plays a role in orchestrating defence mechanisms against biotrophic pathogens, which derive nutrients from living host tissues (Glazebrook, 2005). Upon pathogen detection, SA synthesis is rapidly upregulated, leading to the reprogramming of the plant's transcriptome to initiate defence responses (Zhou & Zhang, 2020). SA is perceived by two classes of receptors, NPR1 and NPR3/NPR4 (Spoel & Dong, 2024). The binding of SA to NPR1 or NPR3/NPR4 have opposing roles in regulating the transcription of SA-associated defence genes (Figure 3; Ding et al., 2018). At low SA concentrations, NPR1 is found in the cytoplasm as an oligomer. Upon pathogen infections and subsequent increase in SA levels, redox changes trigger the monomerization of NPR1, allowing it to localise to the nucleus (Verma et al., 2016). In the nucleus NPR1 acts as a transcriptional coactivator, allowing TGA transcription factors (TFs) to promote the transcription of SA-responsive defence genes. Conversely, NPR3/NPR4 serves as transcriptional co-repressors by binding TGA TFs when SA is absent. The presence of SA disrupts this binding, enabling NPR1 to interact with TGA TFs (Ding et al., 2018). Moreover, increases in SA concentrations induce the expression of pathogenesis-related (PR) genes, including PR1, PR2, and PR5, which are involved in reinforcing plant defence (Koo et al., 2020). Furthermore, increased SA levels enhance both local and systemic acquired resistance (SAR), providing broad-spectrum protection against various microbial pathogens (Verma et al., 2016), a feature analogous to the innate immune system in animals. In addition to its direct role in defence, SA also modulates the production of other defence hormones and signalling molecules, such as reactive oxygen species (ROS), which are crucial for amplifying the immune response (Spoel & Dong, 2024).

JA, on the other hand, is primarily associated with defence against necrotrophic pathogens, which kill and feed on dead plant tissues, and herbivorous insects (Glazebrook, 2005). JA regulates a wide range of physiological processes, including germination, senescence, fruit ripening, and responses to both biotic and abiotic stresses (Koo et al., 2020). Although SA and JA often function antagonistically, where the activation of one can suppress the other's signalling pathways, their coordinated action is essential for mounting an effective defence response (Koo et al., 2020). The interplay between SA and JA allows plants to tailor their immune responses based on the type of

pathogen encountered, ensuring optimal defence while minimising resource expenditure (Verma et al., 2016). Understanding the intricate regulation and interactions of SA and JA signalling pathways not only highlights the complexity of plant immune systems but also underscores the importance of these hormones in maintaining plant health and resilience against a wide range of environmental challenges.

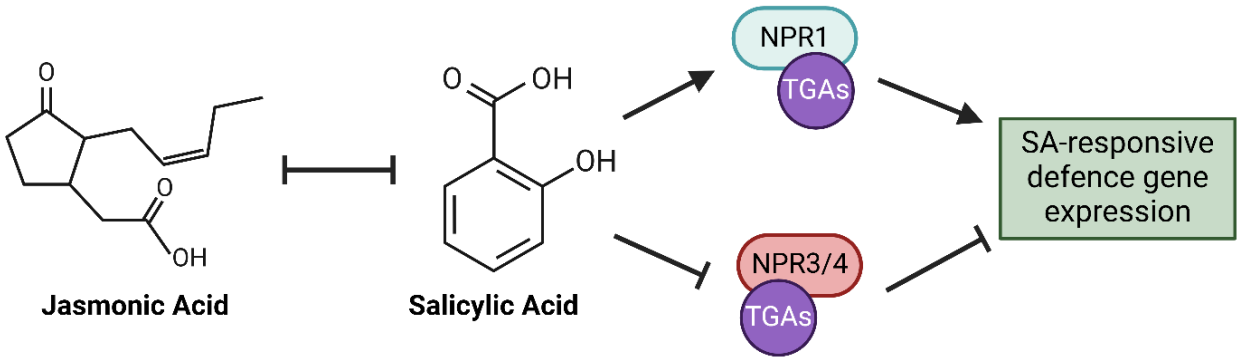

Figure 3. Regulation of SA-responsive defence gene expression. Jasmonic acid and salicylic acid have antagonistic activity. SA activates NPR1 which then activates SA-responsive defence genes. NPR3/4 act as repressors of SA-responsive defence gene expression. Both NPR1 and NPR3/4 partner with TGA transcription factors. Adapted from Ding et al., 2018 and Zhou & Zhang, 2020. Created with BioRender.com

1.3.2 Flg22

Flg22, a well-studied microbe-associated molecular pattern (MAMP), is a conserved 22-amino acid peptide derived from the N-terminus of bacterial flagellin (Yamaguchi & Kawasaki, 2021). This peptide plays a crucial role in the plant immune response by acting as a potent elicitor of plant defences. The recognition of Flg22 by plant cells is mediated through pattern recognition receptors (PRRs), specifically the receptor-like kinase FLS2 (Flagellin-Sensing 2) located on the plasma membrane (Boller & Felix, 2009; Chinchilla et al., 2006). Plants recognize MAMPs in the apoplast to initiate immune responses (Pengpeng Lü et al., 2022). Upon Flg22 perception, FLS2 forms a complex with another receptor-like kinase, BAK1 (BRI1-Associated Receptor Kinase 1), leading to the phosphorylation of both receptors (Sun et al., 2013). Upon recognition of Flg22 by the FLS2-BAK1 receptor complex, a series of rapid and extensive transcriptional changes occur in the plant cell to mount an effective immune response (Macho & Zipfel, 2014). These changes are mediated by a complex network of signalling pathways, leading to the activation of numerous

defence-related genes (Zhou & Zhang, 2020). The early signalling events include the production of reactive oxygen species (ROS), which further serve as signalling molecules to amplify the immune response (Bigeard et al., 2015), as well as the activation of mitogen-activated protein kinases (MAPKs) (Macho & Zipfel, 2014). The MAPK cascade leads to the phosphorylation and activation of transcription factors that induce the expression of defence-related genes (Asai et al., 2002). Finally, the ability of Flg22 to elicit strong immune responses makes it a valuable tool for studying plant immunity and understanding the molecular mechanisms underlying PRR-mediated signalling (Boller & Felix, 2009; Jelenska et al., 2017). Research has shown that Flg22 not only triggers local immune responses but also enhances systemic acquired resistance (SAR), providing long-lasting protection against secondary infections (Jelenska et al., 2017; Yamaguchi & Kawasaki, 2021; Zhou & Zhang, 2020).

1.4 Ribosome inactivating proteins

1.4.1 General overview

Ribosome inactivating proteins (RIPs) are a class of *N*-glycosylases with a distinctive capability to hydrolyse purine bases from ribonucleic acid (RNA) (Marchant & Hartley, 1995; Karran & Hudak, 2008; Fabbrini et al., 2017; Zhu et al., 2018). Specifically, RIPs cleave the N-glycosidic bond linking adenine bases from the ribose phosphate backbone of RNA, a process known as depurination. This depurination event primarily targets the ribosomal RNA (rRNA) at the highly conserved α-sarcin/ricin loop (SRL) of the large ribosomal subunit (Figure 4; Endo & Tsurugi, 1988). The consequential inactivation of ribosomes disrupts the GTP-dependent binding of elongation factor 2/G, thereby impeding the translation elongation process and ultimately inhibiting protein synthesis (Irvin, 1983; Montanaro et al., 1975; Osborn & Hartley, 1990). While RIPs predominantly depurinate ribosomal RNA, their enzymatic activity extends beyond rRNA, including diverse polynucleotide substrates such as supercoiled DNA, mRNA, poly(A) and viral RNA (Barbieri, 1997; Hudak et al., 2002; Rajamohan et al., 1999a; Gandhi et al., 2008). Notably, the antiviral potential of RIPs against both animal and plant viruses has garnered significant attention, as they have demonstrated the ability to inhibit viral RNA translation through depurination (reviewed in Citores et al., 2021 and Kumar et al., 2021). Furthermore, RIPs have been shown to be inducible by a range of abiotic and biotic stresses as well as plant hormones such as abscisic acid (ABA), JA and SA (Chuang et al., 2013; Iglesias et al., 2005; Qin et al., 2009; Song et al., 2000; Zhu et al., 2018). Nevertheless, the precise regulatory mechanism that controls

endogenous RIP expression and their specific integration within stress response pathways remains elusive.

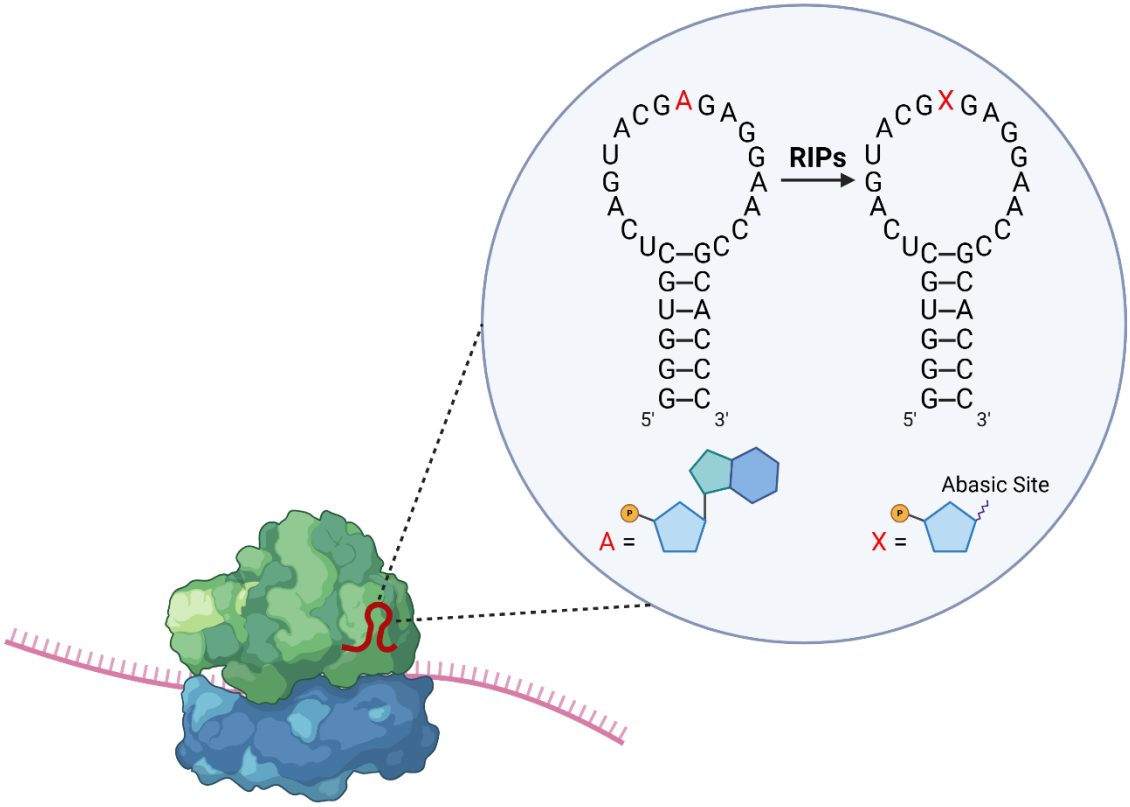

Figure 4. SRL depurination by RIPs. The sarcin ricin loop is indicated in red on the large ribosomal subunit. The bubble takes a closer look at the depurination caused by RIPs. The targeted adenine is coloured in red. A schematic of the adenine base is below the sarcin ricin loop. Depurination of the red adenine leaves an abasic site on the SRL, leading to ribosome inactivation. Created with BioRender.com

1.4.2 Pokeweed Antiviral Protein (PAP)

Pokeweed Antiviral Protein (PAP), derived from the American pokeweed plant (*Phytolacca americana*), is a notable member of the RIP family. Despite pokeweed not being a model organism, its genome has been sequenced and transcriptome experiments under various stress conditions have been conducted (Neller et al., 2019; Dougherty et al., 2024). Within the pokeweed genome, multiple PAP isoforms are encoded by distinct genes. While PAP-I represents

the first and most extensively studied isoform (Irvin, 1975), other detected isoforms include PAP-II, PAP-α, PAP-S1, PAP-S2, and a novel PAP variant (Neller et al., 2019). All PAP isoforms feature an N-terminal sequence guiding protein translation to ribosomes positioned on the surface of the endoplasmic reticulum (ER), thereby facilitating entry of the translated protein product into the ER lumen (Barbieri et al., 1993). The maturation of PAP involves post-translational proteolytic processing of the N- and C-termini, ultimately yielding a 29 kDa mature protein. The functional significance of the processing of the C-terminal end of the protein remains unknown. Moreover, PAP contains the conserved RIP amino acids within its active site, including arginine and glutamic acid responsible for depurination activity, along with valine and serine, which contribute to stabilising the adenine base (Figure 5; Shi et al., 2016; Prashar et al., 2023).

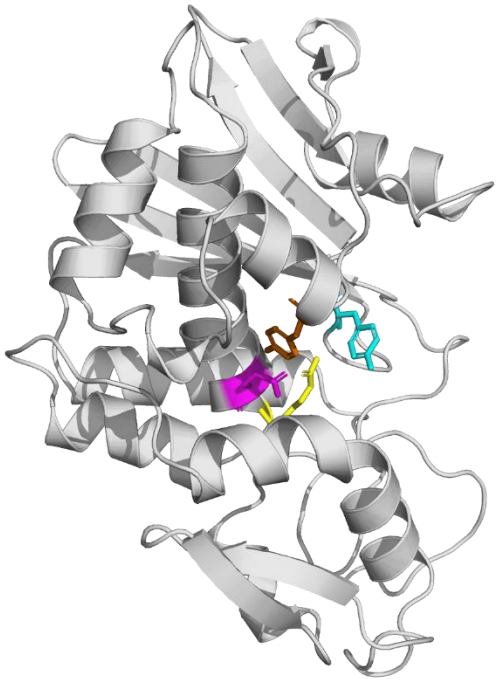

Figure 5. Cartoon representation of the 3D structure of mature PAP. The 3D structure of PAP was obtained from the AlphaFold Protein Structure Database (Jumper et al., 2021; Váradi et al., 2023). The structure of the mature form of PAP is coloured in grey (without the N- and C-terminal sequences). The residues of the PAP active site are coloured as follows: tyrosine (Y72) in cyan, tyrosine (Y123) in orange, glutamic acid (E176) in pink, and arginine (R179) in yellow.

The predominant localization of PAP within the apoplastic space suggests an alternate functionality beyond its known interaction with ribosomes (Ready et al., 1986). PAP has been reported to comprise 0.5% of total soluble proteins in pokeweed leaf tissue (Bonness et al., 1994).

Transcriptome analyses revealed a significant upregulation of multiple PAP genes in response to jasmonic acid (JA) (Neller et al., 2019), emphasising their potential involvement in defence mechanisms. In 1925, Duggar and Armstrong observed a reduction in tobacco mosaic virus (TMV) infectivity in tobacco leaves following the application of soluble extracts from pokeweed leaves (Duggar & Armstrong, 1925). Although the specific RNA structural features essential for PAP's antiviral activity remain elusive (Hudak et al., 2000; Vivanco and Tumer, 2003), emerging evidence indicates its capacity to directly target the genomes of both animal and plant RNA viruses, disrupting critical stages in their life cycles (He et al., 2008; Karran and Hudak, 2008; Mansouri et al., 2009; Krivdova & Hudak, 2015). PAP-I has demonstrated depurination activity against various animal viruses including influenza (Tomlinson et al., 1974), poliovirus (Ussery et al., 1977), herpes simplex virus (Aron & Irvin, 1980), and genomic HIV-1 RNA (Rajamohan et al., 1999a; Rajamohan, et al., 1999b; Uckun et al., 2003). Its antiviral properties have also been demonstrated for economically significant plant viruses, such as TMV (Chen et al., 1993), brome mosaic virus (BMV) (Picard et al., 2005), tobacco etch virus (TEV) (Domashevskiy et al., 2012), cucumber mosaic virus (CMV) (Tomlinson et al., 1974), potato virus X and Y (PVX and PVY) (Lodge et al., 1993). Despite these findings, the antiviral activity of PAP-I and its role in plant defence within its endogenous environment remains unknown.

1.5 Research objectives

Currently, our understanding of PAP protein interactions is limited, with ribosomal proteins being the primary known interactors. However, recent research conducted by a former graduate student in our lab has revealed a potential interaction between PAP and a putative cysteine protease, as identified through immunoprecipitation and mass spectrometry. The objective of my research is to characterise this newly discovered cysteine protease in pokeweed and elucidate its interaction with PAP. My primary focus is to verify whether the identified pokeweed protein functions as a cysteine protease and assess its enzymatic activity. Additionally, I will confirm the binding between this protein and PAP, determine its subcellular localization, and investigate the consequences of its interaction with PAP. I hypothesise that this interaction may lead to the inhibition of either protein's activity or potentially involve proteolytic processing of PAP by the cysteine protease, thereby impacting PAP's function.

2. MATERIALS AND METHODS

2.1 Plant Cultivation

2.1.1 *Phytolacca americana*

Phytolacca americana (pokeweed) seeds were provided by the Tumer laboratory at Rutgers University, NJ (USA) and have been grown and maintained at York University, ON (Canada). To assist with germination, seeds were covered in sulphuric acid and rotated for 5 minutes and rinsed under running water for 10 minutes. The seeds were then submerged in water for 10 to 12 days, with the water being changed everyday, until about 90% of the seed coats were visibly cracked. The seeds were sown in individual square 2 inch pots containing soil mix (1-part garden soil: 1-part Pro-mix all-purpose soil: 0.5-part cattle manure: 0.5-part sand). The trays containing the individual pots were placed on an electric heat pad and covered with clear plastic domes to aid in germination speed and maintain humidity until cotyledons fully emerged.

2.1.2 *Nicotiana benthamiana*

Nicotiana benthamiana (tobacco) seeds were originally obtained from Tumer laboratory at Rutgers University, NJ (USA). The seeds were sown directly in the aforementioned soil mix and grown for 21 days under a plastic dome. Individual seedlings were then transplanted into individual square 2 inch pots and grown for another 14 days under a plastic dome, after which the dome was removed.

2.1.3 Growth conditions

All pokeweed and tobacco plants were grown in growth chambers and were given a 14 hour light/10 hour darkness light cycle. The chamber lighting consisted of 75% fluorescent and 25% incandescent bulbs (180 $\mu E/m^2/s$). The temperature was held at 24°C during the light period and 21°C during the dark period and the fan speeds were set at 65%. The plants were watered approximately every 2 days and fertilised weekly with 20:20:20 (NPK) fertiliser.

2.1.4 Leaf harvest

All pokeweed and tobacco plant tissue used for the subsequent methods (unless otherwise stated) were harvested at the 6 to 8 leaf stages. The leaves without their midvein were stored in a 50 mL conical tube, flash frozen in liquid nitrogen and stored at -40°C until further processed.

2.2 Bioinformatic analysis of PAP interactor

2.2.1 Identification of homologous proteins

The previously performed mass spectrometry analysis identified the pokeweed protein with gene ID anno1.g16742 as the PAP interactor. The amino acid sequence was inputted into Blastp and searched against the Embryophyta clade in the SWISS-PROT database for annotated proteins exclusively. Hits with expected values (E-value) below 1 x 10^{-4} were considered significant to ensure that homologous proteins shared a relation with the query sequence with an error rate below 0.01%. The top scoring protein hit was used to annotate the pokeweed protein. Subsequently, the subcellular localizations and biological functions of the pokeweed protein were annotated, using information from homologous proteins sourced from the UNIPROT database (Bateman et al., 2020).

2.2.2 *In silico* analysis of PaCP1

An InterProScan (v. 5.67; Jones et al., 2014) search was performed to identify protein domains, protein superfamily, and the active site encoded by the PaCP1 amino acid sequence. The global alignment of AtXCP1 and PaCP1 was performed using Blastp. Signal-P (v. 6.0; Teufel et al., 2022) and Target-P (v. 2.0; Almagro Armenteros et al., 2019) were used to confirm the presence of the signal peptide. DeepLoc (v. 2.0; Thumuluri et al., 2022) was used to predict the subcellular localization of PaCP1 using its amino acid sequence.

2.2.3 AlphaFold protein structure prediction modelling

The PaCP1 structural prediction was generated using the open source colab implementation of AlphaFold2 using the default settings (Jumper et al., 2021; Mirdita et al., 2022). The PAP-PaCP1 interaction structural predictions were generated using the open source colab implementation of AlphaFold multimer using the default settings (Evans et al., 2021). The generated structures were then formatted in PyMol to colour different proteins and their domains, as well as to highlight the amino acid residue of the active site.

2.3 Generation of His-tagged PaCP1 clone

2.3.1 Total RNA isolation

Leaf tissue from healthy pokeweed plants had their mid vein removed, were flash frozen in liquid nitrogen, and stored at -40°C until further processing. No more than 100 mg of frozen tissue was homogenised using a chilled mortar and pestle and total RNA was extracted with the

Monarch Total RNA Miniprep Kit (New England Biolabs #T2010) according to the manufacturer's protocol, except that samples were eluted with 75 µL of dH_2O instead of 100 µL. In-column DNAse treatment was performed according to the manufacturer's instructions. RNA concentration was measured using a spectrophotometer (A_{260} nm) and RNA quality was evaluated by separating approximately 500 ng of sample on a 1% agarose gel at 100 V for 20 minutes.

2.3.2 Reverse Transcription (RT)

Total pokeweed RNA (500 ng) was combined with 1 µL of 10 µM gene specific reverse primer to a final volume of 10 µL and denatured at 65°C for 10 minutes. Following denaturation, samples were cooled on ice for 2 minutes and mixed with Mashup reverse transcriptase (Alekseenko et al., 2021) master mix which contained the following components: 0.5 µL of purified Mashup reverse transcriptase, 20 units of murine RNase inhibitor (New England Biolabs #M0314), 4 µL of 5X First Strand Buffer (375 mM KCl, 15 mM $MgCl_2$, 250 mM Tris-HCl pH 8.3), 1 µL of 0.1 M DTT, 1 µL of 10 mM dNTPs, and dH_2O to a final volume of 10 µL. Samples (20 µL) were incubated at 50°C for 60 minutes, followed by heat inactivation of the RT enzyme at 70°C for 10 minutes. cDNAs were stored at -20°C until further processed.

2.3.3 PCR for cloning

PCR was used for amplification of DNA fragments for cloning. 1 µL of RT product (generated in section 2.3.2) was used as a template. The primers used to amplify the fragments during PCR introduced restriction enzyme cut sites corresponding to those present in the pET28a vector at the appropriate sites (all primers are listed in Table 2). All 25 µL PCR reactions contained the following components: 5 µL of 5X Q5 buffer (New England Biolabs #B9027), 1.25 µL of 10 µM forward primer, 1.25 µL 10 µM reverse primer, 0.5 µL 10 mM dNTPs, 0.25 µL Q5 High-Fidelity DNA polymerase (New England Biolabs #M0491), 5 ng plasmid template, and dH_2O. PCR amplification was carried out using an ep gradient S thermocycler (Eppendorf AG) with the following settings: 60 second initial denaturation at 98°C; followed by 40 cycles with a 15 second denaturation at 98°C, a 30 second annealing step at primer specific temperature, and an extension step at 72°C for 60 seconds per kb of DNA. The cycles were followed by a final 2 minute extension step at 72°C. The PCR products (5 µL) were visualised on a 1.5% agarose gel to check for correct size of product amplification. The PCR products were then pooled and subject to PCR clean up described in section 2.3.4.

2.3.4 PCR clean-up

PCR products generated in section 2.3.3 were purified to remove any PCR reaction components. All PCR reactions were combined into a single microcentrifuge tube. Equal volume of basic phenol:chloroform:isoamyl alcohol (25:24:1, pH 8.0) (basic PCI) was added, vortexed for 30 seconds and centrifuged at 16,000 x g for 15 minutes. The upper aqueous layer was removed and added to a new tube along with 2.5 volumes of 100% ethanol, 0.1 volume of 3 M NaOAc and 3 µL of linear acrylamide. The DNA fragment was left to precipitate at -20°C overnight. Following incubation, the fragment was pelleted by centrifuging at 16,000 x g for 30 minutes at 4°C. The pellet was washed with 300 µL of 70% ethanol and resuspended in 20-50 µL of dH_2O depending on pellet size. The DNA concentration was measured using a spectrophotometer (A_{260} nm).

2.3.5 Digestion with EcoRI and BlpI

The plasmid backbone used for the generation of HIS-PaCP1 was the bacterial pET28a (Millipore Sigma #69864) expression vector where the inserted genes are under the control of the T7 lac promoter. The genes can also be expressed with an N-terminal or a C-terminal 6xHIS tag. The plasmid also encodes the lacI repressor protein gene for the lac operon system and expresses a kanamycin resistance gene. The pET28a vector and PaCP1 PCR product were subjected to a digestion reaction with EcoRI (New England Biolabs #R3101) and BlpI (New England Biolabs #R0585) restriction enzymes. These restriction sites allow for the removal of the C-terminally expressed 6x-HIS tag from the backbone. The digestion reaction contained the following components: 20 µg of pET28a plasmid DNA or 100 µL of PaCP1 PCR product, 20 units of EcoRI, 10 units of BlpI, 12 µL 10x rCutsmart buffer (New England Biolabs #B6004S) and dH_2O up to a total volume of 120 µL. The reaction was incubated for 2 hours at 37°C. After the initial incubation, an additional 20 units EcoRI and 10 units BlpI was added, and the reaction was incubated for another 2 hours at 37°C. The digested DNA was loaded onto a 1% low-melt agarose gel and was purified using the described method in section 2.6.2.

2.3.6 Ligation of inserts to vector

Digested PaCP1 and pET28a vector in the ratio of 2:1 was mixed with 400 units of T4 DNA ligase (New England Biolabs #M0202), 1 µL 10x T4 DNA ligase buffer (500 mM Tris-HCl pH 7.5, 100 mM $MgCl_2$, 10 mM ATP, 100 mM DTT, pH 7.5) and dH_2O up to a total volume of 10 µL. The ligation reaction was incubated overnight at 16°C. A ligation reaction with no insert was also incubated as a negative control. After incubation, the ligation reactions were transformed into

chemically competent DH5α *E. coli* cells using the method described in section 2.6.4. The plasmids were isolated from single *E. coli* colonies as per the method described in section 2.6.5. Plasmid DNA concentration was measured using a spectrophotometer (A_{260} nm) and subjected to a digestion with EcoRI and BlpI. The samples were separated on a 0.8% agarose gel to check for correct insertion size. Correct insertion of the PaCP1 sequence was verified by Oxford Nanopore Technologies sequencing by Plasmidsaurus (USA).

2.4 Expression and isolation of His-tagged PaCP1 in *E. coli*

2.4.1 LOBSTR *E. coli* transformation

500 ng of plasmid DNA was added to 100 µL of thawed chemically competent LOBSTR (Low Background Strain) *E. coli* cells and the mixture was incubated on ice for 30 minutes. The cells were then heat shocked at 42°C for 40 seconds followed by a 2 minutes cooling period on ice. Next, 400 µL of LB was added and the cells were incubated horizontally at 37°C for 1 hour with shaking at 250 rpm. The cells were then pelleted by centrifuging at 16,000 x g for 1 minute. 400 µL of supernatant was removed and the cells were plated on LB agar plates with chloramphenicol (35 µg/mL) and kanamycin (50 µg/mL) and incubated at 37°C overnight.

2.4.2 Protein isolation

Transformed LOBSTR cells were grown in 5 mL LB medium at 37°C overnight, supplemented with chloramphenicol and the appropriate plasmid-based antibiotic selection. 4 mL of the saturated culture was transferred to 250 mL LB with the necessary antibiotics and incubated at 37°C until the optical density (OD_{600}nm) reached 0.8. Induction was initiated by introducing IPTG at a final concentration of 0.6 mM and the culture was transferred to an 18°C shaking water bath in a cold room for 16 hours. Following this, the culture was centrifuged at 10,000 x g for 20 minutes at 4°C. The resulting cell pellet was either stored at -20°C or directly used in the following lysis step.

2.4.3 Disruption via sonication

The cell pellet was resuspended in 10 mL of lysis buffer (50 mM Tris pH 8.0, 300 mM NaCl, 5% glycerol) and subjected to sonication (10 seconds ON; 30 seconds OFF) at a peak-to-peak amplitude of 18 microns for 25 cycles, depending on the size of the culture (more sonication is needed for a larger cell count). The lysate was then subjected to centrifugation at 10,000 x g for

30 minutes at 4°C. The supernatant, containing the soluble components, was filtered through a 0.22 µm syringe filter to eliminate potential debris that did not precipitate during centrifugation.

2.4.4 Purification via nickel column

500 µL of 1:1 nickel sepharose bead slurry (GE Healthcare #175318-01) in 20% ethanol was layered on the column bed of 5 mL propylene gravity columns (Thermo Fisher Scientific #29922). The column was washed once with 5 mL of dH_2O, then 5 mL of lysis buffer and was emptied by gravity flow. The supernatant was applied to the column followed by a 30 mL wash of 1 mM imidazole in lysis buffer followed by a 30 mL wash of 25 mM imidazole in lysis buffer. The purified was eluted from the column with 6 mL of 250 mM imidazole in lysis buffer.

2.4.5 Column concentration

The column-based concentration method allows for buffer exchange and protein concentration. The Amicon Ultra-15 centrifugal filter unit concentrator (UFC901008) with a 10kDa cutoff was used so that the heavier proteins were retained. The concentrator was initially washed with 10 mL of dH_2O and centrifuged at 3000 x g for 15 minutes at 4°C, until the volume reached approximately 1 mL. The eluted protein from the nickel purification step was introduced into the concentrator and underwent centrifugation following the same protocol. Subsequently, 10 mL protein storage buffer (20 mM Tris-HCl pH 8.0, 1 mM EDTA, 1 mM DTT, 100 mM NH_4Cl, without glycerol) was added to the concentrator and centrifuged. This process was repeated four more times to reduce the imidazole content from the elution step. After buffer exchange, the protein was concentrated to 500 uL and transferred to a fresh microcentrifuge tube. An aliquot was separated through 12% SDS-PAGE along with BSA standards (1, 0.5, 0.25, 0.125 and 0.06 µg) and stained with Coomassie to visualise protein bands and assess the quality of purification. The concentration of purified PaCP1 was estimated by comparison to the BSA standard bands. The remaining PaCP1 was aliquoted and stored at -80°C.

2.5 Enzymatic Activity Assays

2.5.1 Determining optimal pH for PaCP1 enzyme activity

The fluorescent protease enzymatic activity assays were performed according to the manufacturer's protocol (Thermo Fisher Scientific #23267) with the following modifications. For the determination of the pH for optimal proteolytic activity, buffers at different pHs were used. For pH 4, 4.5, 5, 5.5, and 6, FTC-Casein and purified PaCP1 were diluted in 0.1 M sodium citrate

buffer, while for pH 6.5, 7, and 7.5 they were diluted in 50 mM MOPS buffer. The purified PaCP1 was diluted to a concentration of 1 µg/mL and this was the working concentration for all future enzymatic activity assays. 100 µL of 1 µg/mL purified PaCP1 was added to a black 96-well plate along with 100 µL of FTC-Casein working reagent (10 µg/mL; 1:500 dilution of 5 mg/mL stock). Blank control samples were also made using 100 µL of buffer only (at working pH) and 100 µL of FTC-Casein working reagent. This was repeated three times on the same plate to serve as technical replicates for each pH. The plate was then wrapped in tinfoil and incubated in the dark for 3 hours at room temperature. Fluorescence values were measured at room temperature using a Synergy H4 Hybrid microplate reader using excitation at 485 nm and emission at 538 nm. Proteolytic activity was measured as relative fluorescence units (RFU). RFU values were obtained by subtracting fluorescence measurements of blank controls from those of experimental samples (RFU = experimental - blanks). This assay was independently repeated three times for each pH.

2.5.2 Enzyme inhibition assay

The enzymatic inhibition assays were performed based on the fluorescent protease enzymatic activity assays described above in section 2.5.1 with the following modifications. After determining that PaCP1 was most active at pH 6, all subsequent dilutions (for PaCP1, FTC-Casein and Papain) were performed using 0.1 M sodium citrate buffer pH 6. To test enzymatic inhibition, 100 µL of purified PaCP1 or 1 µg/mL papain (Millipore Sigma #P5306) was added along with 100 µM of E-64 (Thermo Fisher Scientific #78434). This was incubated at room temperature for 30 minutes and was followed by the addition of 100 µL of FTC-Casein working reagent (same concentration as in section 2.5.1). This was repeated three times on the same plate to serve as technical replicates. This assay was also independently repeated three times. The plate was then wrapped in tinfoil and incubated in the dark for 3 hours. Fluorescence values were measured using the same setup as described in section 2.5.1.

2.5.3 Effects of PAP on PaCP1 activity

To test the effects of PAP on PaCP1's enzymatic activity, a modified version of the enzyme inhibition assay described above was used (section 2.5.1). 100 µL of 1 µg/mL purified PaCP1 was added to a black 96-well plate along with varying concentrations of purified PAP-1 protein (previously purified by a Hudak Lab alumni). Three concentrations of PAP-1 were tested, 1 µg/mL, 10 µg/mL, and 100 µg/mL, thereby testing a 1:1, 1:10, and 1:100 ratio of PaCP1 to PAP protein. PaCP1 and PAP were incubated for 30 minutes at room temperature followed by the addition of

100 µL of FTC-Casein working reagent (same concentration as in section 2.5.1). This was repeated three times on the same plate to serve as technical replicates. This assay was also independently repeated three times. The plate was then wrapped in tinfoil and incubated in the dark for 3 hours. Fluorescence values were measured using the same setup as described in section 2.5.1.

2.5.4 Enzyme kinetics assay

To assess the rate of PaCP1's enzymatic reaction, a modified version of the enzyme activity assay was used (section 2.5.1). 0.1 µg of purified PaCP1 (100 µL of 1 µg/mL) PaCP1 was added to a black 96-well plate along with varying concentrations of FTC-Casein (0.3125, 0.625, 1.25, 2.5, 5, 10, 20, 40 µM). The reaction was incubated at 22°C for 1 hour. Fluorescence values were measured using the same set up as described in section 2.5.1. GraphPad prism 10 was used to determine the V_{max} and the K_m values using the Michaelis-Menten method.

2.6 Confirming PAP-PaCP1 interaction by yeast two-hybrid

2.6.1 attB adapter PCR

The attB-PCR products were generated according to the manufacturer's protocol (Thermo Fisher Scientific #12536017). Briefly, two PCR reactions were used for the amplification and generation of DNA fragments with attB1 (5') and attB2 (3') sites. The primers for the first PCR reaction were designed by including half of the attB1 or attB2 sequence along with a gene-specific sequence. The primers for the second PCR amplification contained the full attB1 and attB2 sequence. All primer sequences are listed in Table 2. All 25 µL PCR reactions contained the following components: 5 µL of 5X Q5 buffer (New England Biolabs #B9027), 1.25 µL of 10 µM forward primer, 1.25 µL 10 µM reverse primer, 0.5 µL 10 mM dNTPs, 0.25 µL Q5 High-Fidelity DNA polymerase (New England Biolabs #M0491), 1 µL attB PCR products, and dH_2O. PCR amplification was carried out using an ep gradient S thermocycler (Eppendorf AG) with the following settings: 60 second initial denaturation at 98°C; followed by 40 cycles with a 15 second denaturation at 98°C, a 30 second annealing step at primer specific temperature, and an extension step at 72°C for 60 seconds per kb of DNA. The cycles were followed by a final 2 minute extension step at 72°C. The PCR products (5 µL) were visualised on a 1.5% agarose gel to check for correct size of product amplification. The attB-PCR products were then purified using low-melt agarose gel extraction as described in section 2.6.2.

2.6.2 Low-melt agarose gel extraction

The DNA was loaded onto a precast 1% low-melt agarose with 4 µL of Midori Green dye (Nippon Genetics #MG10) and separated for 90 minutes at 80V. A handheld blue light with a 510/520 nm bandpass filter was used to view the DNA fragments. The desired DNA fragment was then excised and extracted using 100 µL of 2x elution buffer (20 mM Tris-HCl pH 8, 400 mM NaCl, 2.5 mM EDTA) per 100 mg of agarose and heated at 65°C for 30 minutes to melt the agarose. Once melted, equal volume of phenol (pH 8) was added, vortexed for 30 seconds, and centrifuged at 16,000 x g for 15 minutes. The top layer of the supernatant was transferred to a new tube with an equal volume of basic phenol:chloroform:isoamyl alcohol (25:24:1, pH 8). The mixture was vortexed for 30 seconds and centrifuged at 16,000 x g for 15 minutes. The upper aqueous layer was transferred to a new tube along with 2.5 volumes of 100% ethanol, 0.1 volume of 3 M NaOAc and 5 µL of linear acrylamide (Thermo Fisher Scientific #AM9520). The DNA was left to precipitate at -20°C overnight. Following precipitation, the DNA was pelleted by centrifugation at 16,000 x g for 30 minutes at 4°C. The pellet was then washed with 500 µL of 70% ethanol and resuspended in 20-50 µL of dH_2O depending on pellet size. DNA concentration was quantified using a spectrophotometer (A_{260} nm).

2.6.3 Generation of entry clone by Gateway™ cloning BP recombination reaction

The BP recombination reaction between attB-PCR products and pDONR221 (Thermo Fisher Scientific #12536017) was performed according to the manufacturer's protocol. Briefly, 150 ng of attB-PCR products and 150 ng of pDONR221 were mixed with 2 µL of BP Clonase II enzyme mix (Thermo Fisher Scientific #11789100) and TE buffer pH 8.0 (10 mM Tris-HCl pH 8.0, 1 mM EDTA) to a final volume of 10 µL. The reaction was incubated at 25°C for 18 hours. After the incubation, the reaction was terminated by the addition of 1 µL of Proteinase K (2 µg/µL) and a final incubation at 37°C for 10 minutes. 2 µL of the BP recombination reaction was used to transform DH5α *E. coli* cells as per the method described in section 2.6.4.

2.6.4 DH5α *E. coli* plasmid transformation

2 µL (approximately 500 ng) of plasmid DNA was added to 100 µL of thawed chemically competent DH5α *E. coli* cells and the mixture was incubated on ice for 30 minutes. The cells were then heat shocked at 42°C for 40 seconds followed by a 2 minute cooling period on ice. Next, 400 µL of LB was added and the cells were incubated horizontally at 37°C for 1 hour with shaking at 250 rpm. The cells were then pelleted by centrifuging at 16,000 x g for 1 minute. 400 µL of

supernatant was removed and the remaining 100 µL of resuspended cells were plated on selective LB agar plates and incubated at 37°C overnight.

2.6.5 Small-scale plasmid isolation (miniprep)

A single *E. coli* colony carrying the plasmid of interest was grown in 5 mL LB with the appropriate selective antibiotic. The cultures were incubated overnight at 37°C with shaking at 250 rpm. The following day, 2 mL of culture was centrifuged at 16,000 x g for 1 minute and the supernatant was discarded. Plasmid DNA was obtained with the Monarch Plasmid Miniprep kit (New England Biolabs #T1010) following the manufacturer's protocol. The DNA concentration was measured using a spectrophotometer (A_{260} nm). All plasmids were sequenced by Oxford Nanopore Technologies sequencing by Plasmidsaurus (USA) to ensure correct and expected plasmid sequence.

2.6.6. Generation of destination clone by Gateway™ cloning LR recombination reaction

The LR recombination reaction between the entry clone generated in section 2.6.3 and the destination vector (pDEST22 or pDEST32) was performed according to the manufacturer's protocol. Briefly, 150 ng of entry clone plasmid and 150 ng of destination plasmid was mixed with 2 µL of LR Clonase II enzyme mix (Thermo Fisher Scientific #11791020) and TE buffer pH 8.0 to a final volume of 10 µL. The reaction was incubated at 25°C for 18 hours. After the incubation, the reaction was terminated by the addition of 1 µL of Proteinase K (2 µg/µL) and a final incubation at 37°C for 10 minutes. 2 µL of the LR recombination reaction was used to transform DH5α *E. coli* cells as per the method described in section 2.6.4.

2.6.7 Small scale yeast transformation

Yeast strain MaV203 (*Saccharomyces cerevisiae*) was streaked on a YPAD agar plate from a glycerol stock and grown for 3 days at 28°C. A single colony was used to inoculate 10 mL of YPAD liquid medium and incubated overnight at 28°C with shaking at 200 rpm. The overnight culture was diluted to an OD_{600} of 0.4 in 50 mL of YPAD and grown for an additional 4 hours until the OD_{600} reached 0.6-0.7. The cells were then pelleted at 2000 x g for 3 minutes at room temperature. The pellet was resuspended in 40 mL of 1X TE buffer (10 mM Tris-HCl pH 7.5, 1 mM EDTA) and pelleted again for 3 mins at 2000 x g at room temperature. The cells were resuspended in 2 mL 1X LiAc/0.5X TE (0.1M LiAc, 5 mM Tris-HCl pH 7.5, 0.5 mM EDTA) followed by a 10 minute incubation at room temperature. 100 µL of resuspended cells was added

to a microtube containing 500 ng of each plasmid (bait and prey) along with 100 µg denatured sheared salmon sperm DNA. 700 µL of 1X LiAc/40% PEG-3350/1X TE (0.1M LiAc, 5 mM Tris-HCl pH 7.5, 0.5 mM EDTA, 40% PEG-3350) was added and the cells were incubated at 28°C for 30 minutes. After incubation, 88 µL of DMSO was added and the cells were heat shocked at 42°C for 7 minutes. The cells were centrifuged at 16 000 x g for 30 seconds and resuspended in 1 mL of 1X TE buffer. The centrifugation was repeated, and the cells were resuspended in 100 µL 1X TE buffer. Finally, the cells were plated on SC selective media lacking leucine and tryptophan (SC -Leu -Trp) and incubated for 3 days at 28°C.

2.6.8 Testing for the interaction

One colony from each co-transformation was added to 25 mL of SC -Leu -Trp and incubated overnight at 28°C with shaking at 200 rpm. The overnight cultures were diluted to an OD_{600} of 0.3 in a total volume of 25 mL of fresh SC -Leu -Trp and incubated for an additional 4 hours (until OD_{600} reached ~0.6). The cells were pelleted at 3000 x g for 3 mins, resuspended, and washed in 2 mL of 0.9% filter sterilised NaCl. The cells were then re-pelleted and resuspended in 1 mL of 0.9% NaCl. To assess the 3-Amino-1,2,4-triazole (3AT) (Sigma #A8056) sensitivity of the interaction, the cells from each transformation pair were serially diluted (10-fold) in a 96 well plate up to a dilution of 10^{-7} (including undiluted). Using a multichannel pipette, 8 µL of each dilution was then plated on SC -Leu -Trp -His plates with increasing concentration of 3AT (0 mM, 10 mM, 25 mM, 50 mM, 75 mM, 100 mM). The plates were incubated for 48 hours at 28°C. To increase the sensitivity of the interaction and eliminate false positives, a 25 mM 3AT concentration was used for the final plate.

2.7 Subcellular localization of PaCP1

2.7.1 Generation of PaCP1-eGFP expression clone

Total pokeweed RNA was isolated using the method described in section 2.3.1. Reverse transcription coupled with PCR using attB primers for the full length nucleotide sequence of PaCP1 (including signal peptide, pro-inhibitory domain and protease) was performed as described in sections 2.3.2 and 2.6.1 to obtain the sequence needed for cloning. Gateway cloning was used to generate a full length PaCP1 entry clone and the final destination vector as described in sections 2.6.3. The full length PaCP1 sequence was cloned in pGWB405 (a Gateway™ compatible binary vector which C-terminally tags the protein of interest with eGFP; Nakagawa et al., 2007) as per

the method in section 2.6.6. As the constructs were cloned using gateway cloning, the empty vector-eGFP construct was cloned by using the PaCP1 nucleotide sequence with the introduction of an early stop codon after the first 21 nucleotides which served as a negative expression control. The constructs were transformed in DH5α *E. coli* as per section 2.6.4 and plasmid DNA was extracted as per the method in section 2.6.5.

2.7.2 *Agrobacterium tumefaciens* transformation

Plasmid DNA (100-150 ng) was added to 100 µL of thawed *Agrobacterium tumefaciens* (Agrobacterium) AGL1 electrocompetent cells and the mixture was transferred into 2 mm cuvettes (BioRad #1652082). Cells were electroporated (2.5 kV, 25 µF capacitance, and 400 Ω resistance) and allowed to recover in 3 mL of non-selective YEP medium for 3 hours at 28°C with shaking at 250 rpm. After recovery, 50 µL of non-pelleted cells were plated on YEP agar plates containing 50 µg/mL carbenicillin and 50 µg/mL spectinomycin (YEP Carb/Spec) and incubated at 28°C for 3 days.

2.7.3 Agroinfiltration in *Nicotiana benthamiana* leaves

Agrobacterium cultures transformed with PaCP1-eGFP or EV-eGFP (empty vector) constructs were used to agroinfiltrate four-leaf stage *Nicotiana benthamiana* leaves. Freshly transformed (< 1.5 weeks) Agrobacterium AGL1 cells were grown overnight at 28°C with shaking at 250 rpm in 5 mL of YEP Carb/Spec liquid medium. Agrobacterium cells that had previously been transformed with a helper component protease (HcPro) plasmid were grown overnight in 5 mL YEP Carb/Kanamycin (50 µg/mL carbenicillin and 50 µg/mL kanamycin). The following day, 50 µL of culture was transferred to 25 mL of YEP Carb/Spec or YEP Carb/Kan medium and incubated with shaking at 275 rpm for an additional 12-14 hours, until late log phase (OD_{600} = 0.7 – 1.2). Cells were pelleted by centrifugation at 3000 x g for 10 minutes and washed with 15 mL of agroinfiltration solution (10 mM MES-KOH, pH 5.6, 10 mM $MgCl_2$, 200 µM acetosyringone). After washing, cells were resuspended in agroinfiltration solution to a final OD_{600} of 0.5 and incubated at room temperature in the dark for 3 hours. Prior to agroinfiltration, cultures transformed with the PaCP1- or EV-eGFP constructs were each mixed in a 2:1 ratio with the HcPro culture. Agrobacterium cells were infiltrated into the abaxial surface of leaves using a needleless 5 mL syringe.

2.7.4 Sample preparation and imaging

At 72 hours post agroinfiltration, epidermal peels from the abaxial surface of the *N. benthamiana* leaves were taken and added to 50% glycerol in dH_2O to induce plasmolysis. A drop of 50% glycerol was added to a glass slide and the epidermal peel was carefully placed on the slide ensuring the peel did not fold onto itself. The GFP fusion protein was detected under epifluorescent microscope (x40) with a Zeiss Axio Observer A1 equipped with a 489 nm excitation and 509 nm emission filter and photographed with a digital camera.

2.8 Co-localization of PAP and PaCP1

2.8.1 Apoplastic fluid extraction

This protocol was adapted and modified from the method of O'Leary et al. (2014). Intact pokeweed leaves had their mid-veins removed and the two halves were further cut in half (4 pieces per leaf). The pieces were rinsed with deionized water to remove the cellular proteins from the cut ends. The leaf pieces were then blotted dry and placed in a 60 mL needleless syringe along with 40 mL of apoplastic infiltration buffer (20 mM ascorbic acid, 20 mM NaCl, pH 4.0). After removal of the air, the opening of the syringe was sealed using a folded piece of parafilm to create an airtight seal. The buffer was infiltrated into the apoplast by pulling the syringe plunger upwards without breaking the vacuum seal. After a 10 second pause in the fully extended position, the plunger was slowly pulled back into the syringe. This was repeated until the leaves had been fully infiltrated which was visualised by their darker, more translucent appearance. The leaves were gently patted dry without disrupting any of the cellular integrity. The leaves were then wrapped in parafilm and inserted into a 15 mL tube with miracloth forming a suspended bag within the tube. The tubes were centrifuged at 2000 x g for 25 minutes at 4°C and apoplastic fluid was collected at the bottom. Apoplastic proteins were dissolved in 2X Laemmli buffer (125 mM Tris-HCl pH 6.8, 4% (w/v) SDS, 20% (v/v) glycerol, 10% (v/v) b-mercaptoethanol, 0.02% (w/v) bromophenol blue) and separated on 12% SDS-PAGE. The presence of proteins of interest was detected by immunoblot analysis (as described in section 2.8.3).

2.8.2 Total protein isolation

Pokeweed and tobacco leaf tissue (0.2 g) were homogenised by grinding in liquid nitrogen using a chilled mortar and pestle. 400 µL of cold protein extraction buffer (50 mM Tris-HCl pH 7.5, 1 mM EGTA, 1 mM DTT, 1x protease inhibitor (Thermo Fisher Scientific #A32963), 5% glycerol) was added. Lysates were transferred to a new 1.7 mL tube and vortexed until

homogenised, incubated for 5 minutes on ice for proteins to solubilize and centrifuged at 10,000 x g for 5 minutes at 4°C to pellet cellular debris and supernatants were transferred to new tubes. A second centrifugation was performed, and supernatants were again transferred to a new tube. Total protein concentration of lysates was measured by Bradford assay.

2.8.3 Immunoblotting

Proteins to be separated by SDS-PAGE were solubilized in equal volume of 2x Laemmli buffer. The proteins were then denatured for 5 minutes at 90°C. Equal µg amounts of protein were loaded onto a 12% gel. The proteins were separated at 200V for 45 minutes in an SDS running buffer (192 mM glycine, 25 mM Tris-HCl pH 8.3, 0.1% SDS). Proteins were then transferred to a nitrocellulose membrane using a wet transfer system at 120V for 25 minutes in transfer buffer (160 mM glycine, 25 mM Tris-HCl pH 8.3, 20% (v/v) methanol, 0.02% SDS). The membrane was then blocked with either 5% milk in PBS-T (PBS with 1% Tween 20) or 5% BSA in TBS-T (TBS with 1% Tween 20) for 2 hours at room temperature with rocking. The blot was then incubated overnight at 4°C with rocking with the appropriate primary antibody in fresh 5% milk in PBS-T or 5% BSA in TBS-T. The next day, the blot was washed 4 times in PBS-T or TBS-T for 10 minutes each at room temperature with rocking. The blot was then incubated for 1.5 hours with rocking at room temperature with 5% milk in PBS-T with the appropriate horseradish peroxidase-conjugated secondary antibody. The blot was then washed again four times in PBS-T for 10 minutes and then once with dH_2O for 5 minutes, all at room temperature with rocking. After washing, 1 mL of luminol reagent and 1 mL of peroxide reagent (Thermo Fisher Scientific #32109) were applied to cover the blot which was then imaged using a MicroChemi imager (DNR Bio-imaging systems).

Table 1. List of antibodies and their corresponding buffers used for immunoblot analysis.

Antibody	Dilution	Buffer used	Supplier and Catalog #
Rabbit Anti-PAP polyclonal	1:10 000	5% milk in PBS-T	Gift from N. Tumer (Rutgers University)
Rabbit Anti-Papain polyclonal	1:500	5% BSA in TBS-T	Bethyl Laboratories #A150-114
Rabbit Anti-Ribosomal Protein uS3 polyclonal	1:1000	5% BSA in TBS-T	New England Biolabs #9538S
Mouse Anti-β-actin monoclonal	1:1000	5% milk in PBS-T	Novus Biologicals #74340

2.9 PAP degradation by PaCP1

2.9.1 Incubation and immunoblotting

To test whether PaCP1 cleaves PAP, 100 ng of purified PaCP1 (purified in section 2.4) was combined with 10 000 ng of purified PAP-1 protein (previously purified by a Hudak Lab alumni) in 0.1 M sodium citrate buffer at pH 6 and incubated at room temperature for 4 hours with shaking at 120 rpm. The proteins were then denatured in equal volume of 2x Laemmli buffer and heated for 5 minutes at 90°C. Subsequently, the proteins were either used for immunoblotting analysis (as described in section 2.8.3) or mass spectrometry analysis as described below.

2.10 Mass spectrometry analysis of PAP degradation products

2.10.1 In-gel reduction and alkylation

Proteins were separated through 12% SDS-PAGE for 40 minutes at 200 V in an SDS running buffer (192 mM glycine, 25 mM Tris-HCl pH 8.3, 0.1% SDS). The gel was stained in Coomassie stain solution (0.1% (w/v) Coomassie blue R250, 50% (v/v) methanol, 10% (v/v) glacial acetic acid) for 1 hour with rocking at room temperature, quickly rinsed two times with water, and then rinsed in water with rocking for 1 hour. Bands were excised with a clean razor blade and then cut into cubes (approx. 1x1 mm). Gel pieces were transferred to a 1.7 mL microtube and briefly spun down. To destain gel pieces, 200 µL of destaining solution (50 mM ammonium bicarbonate (ABC)/acetonitrile (1:1, v/v)) was added to each tube and incubated at 37°C for 30 minutes at 300 rpm. The liquid was removed and the destaining step was repeated a second time. 30 µL of reducing buffer (0.05 M of Tris(2-carboxyethyl)phosphine (TCEP) in 25 mM ABC buffer pH 7.4) was added to the tube, briefly vortexed and incubated at 60°C for 15 minutes. After cooling down the samples to room temperature, the liquid was removed. 30 µL of alkylation buffer (0.1 M iodoacetamide (IAA)) was added and the samples were incubated in the dark for 1 hour at room temperature. The alkylation buffer was removed, and the samples were washed in destaining solution again twice as described above.

2.10.2 In-gel digestion and peptide extraction

To shrink the gel pieces, 50 µL of acetonitrile was added and the samples were incubated at room temperature for 15 minutes. The acetonitrile was removed, and the samples were air dried for 20 minutes. 20 µL of 1% Rapigest SF solution (1 mg Rapigest SF in 100 µL of 25 mM ABC buffer at pH 7.4; Waters #186001860) was added and the samples were incubated for 10 minutes

at 37°C. Trypsin buffer (20 ng/µL trypsin in 10 mM ABC + 10% (v/v) acetonitrile; Promega #V5071) was added to cover gel pieces, and samples were incubated at room temperature for 15 minutes to allow for saturation with the buffer. After 15 minutes, more trypsin buffer was added as necessary to cover gel pieces, followed by the addition of 25 µL of 25 mM ABC and tubes were incubated at 37°C for 4 hours at 300 rpm. The liquid was removed from gel pieces to a new 1.7 mL microtube. Trifluoroacetic acid (TFA)/dH_2O (50/50 v/v) was added to stop the reaction ensuring the pH was below 2. The samples were incubated at 37°C for 30 minutes at 300 rpm, followed by a 10-minute centrifugation at 15, 000 x g. The supernatant was aliquoted and stored at -20°C until further processed.

2.10.3 Mass spectrometry

Mass spectrometry analysis was performed by Maxime Rossato at the mass spectrometry centre (York University) using the TimsToF Pro 2 mass spectrometer (Bruker Daltonics®) coupled to a nanoelut2 LC system (Bruker Daltonics®). Separation of peptides was performed on an analytical column (PepSep Ten Unlimited series, 150 µm x 10 cm, 1.5 µm particle size, 100 Å pore size) using a gradient of solvent A (0.1% formic acid in water) and solvent B (acetonitrile (ACN) with 0.1% formic acid) over 45 minutes from 1 to 35 % B at a flow rate of 500 nL/min with duplicate injection. Data-dependent MS acquisition with PASEF technology in positive mode was achieved with 10 PASEF ramps and a total cycle time of 1.17 s between m/z 100 and 1700, an intensity threshold of 2500 and a target intensity of 20 000 to trigger an MS/MS from a parent ion. TIMS was enabled with $1/K_0$ between 0.6 $V.s.cm^{-2}$ and a collision energy ramping from 20 eV at $1/K_0$ = 0.6 $V.s.cm^{-2}$ to 59 eV at $1/K_0$ = 1.6 $V.s.cm^{-2}$.

2.10.4 Data analysis

Three samples of the 24 kDa and 18 kDa protein products were sent for analysis by mass spectrometry. The peptide list obtained from the mass spectrometry analysis was aligned to the mature PAP-1 sequence using Peptigram (Manguy et al., 2016). The alignments were compared for each of the PAP breakdown products and only the peptides present in two or three of the samples were considered for the analysis.

2.11 Stress treatments of pokeweed plants

2.11.1 Salicylic Acid

Six to eight leaf pokeweed plants were sprayed with 2 mM SA (solubilized in 0.5% ethanol to improve solubility). Plants sprayed with only 0.5% ethanol served as negative controls. Three leaves from each plant were harvested at the following time points: 0, 1, 2, 4, and 6 hours. The leaves were flash frozen in liquid nitrogen and stored at -40°C until further processed. Leaves from three independent plants were pooled together into a single biological replicate. There were three biological replicates for each time point; therefore, nine plants were used per time point.

2.11.2 Flg22

Six to eight leaf pokeweed plants were infiltrated using a needless syringe with 1 µM flg22 (PhytoTech Labs #P6622) solubilized in dH_2O. Plants infiltrated with dH_2O only served as negative controls. Three leaves from each plant were harvested at the following time points: 0, 2, 4, and 6 hours. The leaves were flash frozen in liquid nitrogen and stored at -40°C until further processed. Leaves from three independent plants were pooled together into a single biological replicate. There were three biological replicates for each time point; therefore, nine plants were used per time point.

2.11.3 Quantitative PCR (qPCR)

Total RNA was isolated from frozen leaf tissue using the method described in section 2.3.1. Using the isolated RNA, a reverse transcription step was then performed according to the method in section 2.3.2. The RT reaction products (3 µL) were combined with 2 µL 10 µM forward and 2 µL 10 µM reverse primers, 33 µL of 2X SYBER Green qPCR Master Mix (GeneBio #P2092), and dH_2O to a final volume of 67 µL. Each sample was mixed by pipetting and divided into three 0.2 mL microtubes to make 20 µL technical replicates. qPCRs were conducted in a QIAGEN Rotor-Gene Q thermocycler with the following settings: hold at 50°C for 20 seconds, initial denaturation and hot-start DNA polymerase activation for 10 minutes, followed by 40 cycles alternating between denaturation at 95°C for 15 seconds and combined annealing/extension at 60-66°C for 45 seconds. RNA levels were quantified using the ΔΔCt method (Taylor et al., 2019). The transcript levels of polyA-binding protein and dynamin served as internal controls (Dougherty et al., 2024). Melting curve analyses were performed to ensure that only one PCR product was present for each reaction.

3. RESULTS

3.1 Bioinformatic predictions of putative pokeweed cysteine protease

The pokeweed protein with gene ID anno1.g16742 was previously identified by co-IP and mass spectrometry as a PAP interactor. This protein was identified as a putative cysteine protease through a blastp search of its amino acid sequence against the Embryophyta (land plants) clade in the SWISS-PROT database, based on the highest degree of homology with annotated plant proteins. *Arabidopsis thaliana* xylem cysteine protease 1 (AtXCP1) was the reference sequence with the highest total score (score = 516 and E-value = 0.0) and was used to annotate the pokeweed protein (Figure 6A). Global alignment of the amino acids encoded by the pokeweed gene and AtXCP1 showed 69% identity between the two protein sequences, with 244/355 amino acids conserved (Figure 6A). The pokeweed gene anno1.g16742 will therefore be referred to as *Phytolacca americana* cysteine protease 1 (PaCP1). Using AtXCP1 as the homologous reference sequence, subcellular localization and biological functions of the pokeweed protein were then predicted using information from the UNIPROT database (Figure 6B) (Bateman et al., 2020). Based on these results, PaCP1 is predicted to be localized to the extracellular space and to the vacuole. It is also predicted to play a role in programmed cell death as well as proteolysis in protein catabolism. To further support the inferred identity of PaCP1 as a cysteine protease, an Interproscan search was performed using its amino acid sequence to identify conserved protein regions (Supplemental Figure 1) (Jones et al., 2014). PaCP1 was identified as belonging to the papain-like cysteine peptidases superfamily. Members of this family have been categorized as subfamily C1A, in accordance with the protease-specific database MEROPS (Rawlings & Bateman, 2020). The identified active site comprises cysteine, histidine, and asparagine (C156, H291, N311). This catalytic triad is a characteristic of cysteine proteases (Misas-Villamil et al., 2016). Residues 1-24 were identified as a signal peptide domain, residues 25-132 were identified as a protease inhibitor domain and residues 133-345 were identified as a peptidase C1A domain (Figure 6C). Inhibitor domains are conserved features of cysteine proteases, which are synthesized as inactive precursors. The inhibitor prodomain blocks substrate access to the active site, preventing inappropriate proteolytic activity and unwanted protein degradation (Misas-Villamil et al., 2016). To confirm the presence and cleavage site of a signal peptide, the amino acid sequence was inputted into Signal-P 6.0 and Target-P 2.0 (Teufel et al., 2022; Almagro Armenteros et al., 2019). Both programs identified residues 1-24 as a signal peptide and identified its cleavage

between residue 24 and 25 (Figure 6A, indicated by the white arrow). Furthermore, the cleavage of the inhibitor prodomain was inferred based on sequence homology with AtXCP1 (Figure 6A, indicated by the black arrow). Additionally, the structure of the mature PaCP1 protein (peptidase C1A domain, residues 133-345) was predicted using the colab implementation of AlphaFold2 with default settings (Jumper et al., 2021; Mirdita et al., 2022). Our PaCP1 model was compared to the AtXCP1 model (obtained from the AlphaFold protein structure database; Váradi et al., 2023) and the protein folding was very similar (Figure 6D).

A

```
Score:516 bits(1330), Expect(E-value):0.0,
Identities:244/355(69%), Positives:296/355(83%), Gaps:6/355(1%)

AtXCP1 1    MAFSAPSLSKFSLLVAISASALLCCAFARDFSIVGYTPEHLTNTDKLLELFESWMSEHSK  60
PaCP1  1    MALSLYNLFCFTFTVFHVAYP----ALARDFSIVGYSPDDLSSDEKLHDLFTTWVSKHHK  56

AtXCP1 61   AYKSVEEKVHRFEVFRENLMHIDQRNNEINSYWLGLNEFADLTHEEFKGRYLGLAKPQFS  120
PaCP1  57   FYNSLEEKLLRFELFKDNLKHIDERNKHVSSYWLGLNEFADLSHEEFKNKYLGLRVAQQG  116

AtXCP1 121  RKRQPSANFRYRDITDLPKSVDWRKKGAVAPVKDQGQCGSCWAFSTVAAVEGINQITTGN  180
PaCP1  117  RSKS-SEDFTYREVKSLPKSVDWRKKGAVTPVKNQGSCGSCWAFSTVAAVEGINQIVTGN  175

AtXCP1 181  LSSLSEQELIDCDTTFNSGCNGGLMDYAFQYIISTGGLHKEDDYPYLMEEGICQEQKEDV  240
PaCP1  176  LTSLSEQELVDCDTS-NNGCNGGLMDAAFDFIVSNGGLHKDEDYPYMMEEGHCEQKKEEM  234

AtXCP1 241  ERVTISGYEDVPENDDESLVKALAHQPVSVAIEASGRDFQFYKGGVFNGKCGTDLDHGVA  300
PaCP1  235  DVVTISGHRDVPENDEVSLLKALAHQPLSVGIEASGRDFQFYSGGVFDGHCGTDLDHGVA  294

AtXCP1 301  AVGYGSSKGSDYVIVKNSWGPRWGEKGFIRMKRNTGKPEGLCGINKMASYPTKTK  355
PaCP1  295  AVGFGSTKGSDYIIVKNSWGSRWGEKGYIRMKRNTKRPEGLCGINKMASYPIKKK  349
```

B

Pokeweed Protein	Pokeweed Gene ID	Homologous Protein Name	Homologous Protein Species	Subcellular localization	Biological function
Phytolacca americana cysteine protease 1 (PaCP1)	anno1g.16742	Xylem cysteine protease 1 (XCP1)	*Arabidopsis thaliana*	Extracellular space, vacuole	Programmed cell death, proteolysis in protein catabolism

C

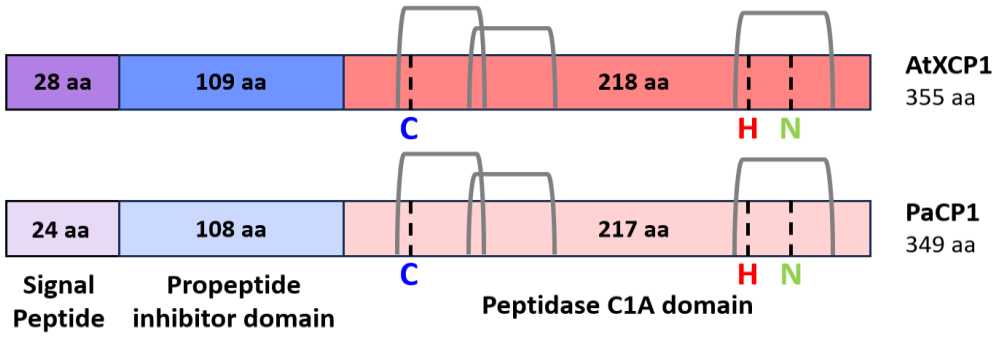

D

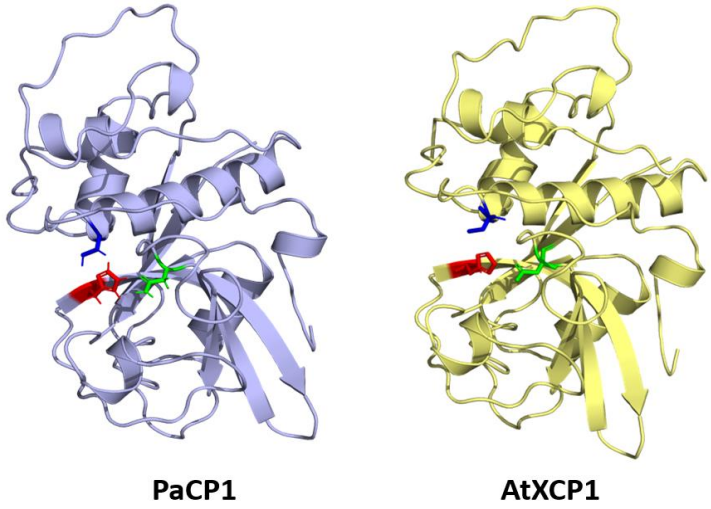

Figure 6. Protein sequence characterization of PaCP1. (A) The amino acid sequence for PaCP1 was aligned to the plant protein sequence with the highest homology, AtXCP1, using blastp. The score, E-value, identities, positives and gaps values are shown at the top. Gray highlights indicate residues that are identical, blue highlights indicate residues with similar chemical properties. Pink residues are required for recognition and cleavage of the signal peptide. Signal peptide cleavage sites for both sequences are indicated by the white arrow. Yellow residues are required for the recognition and cleavage of the propeptide inhibitor domain. The cleavage site of this domain for both sequences is indicated by the black arrow. The residues of the active site are coloured in blue, red and green and represent cysteine (C156), histidine (H291), asparagine (N311), respectively. (B) PaCP1 annotation inferred from homology with AtXCP1. The subcellular localization and biological function were predicted using information from the UniProt database. (C) Comparison schematic of the putative protein sequence organization for PaCP1 compared to the known protein organization of AtXPC1, obtained from UniProt. The location of the signal peptide, propeptide inhibitor domain and peptidase C1A domain for PaCP1 correspond with the results from Interproscan, Signal-P 6.0 and Target-P 2.0. The active site residues responsible for the catalytic activity are presented as follows: cysteine (C; blue), histidine (H; red), and asparagine (N; green), as well as three disulfide bridges shown in grey. (D) Structural prediction of the mature PaCP1 protein (peptidase C1A domain, residues 133-345) using the colab implementation of AlphaFold2. The protein structure of AtXCP1 was obtained from the AlphaFold protein structure database (Jumper et al., 2021; Váradi et al., 2023). The three catalytic residues of the active sites are coloured in the same way as presented in (A and C).

3.2 PaCP1 Enzymatic Activity Assay

To validate the bioinformatic predictions regarding PaCP1 as a cysteine protease from pokeweed, we performed enzymatic activity assays to evaluate its proteolytic capabilities. The mature nucleotide sequence of PaCP1, devoid of the signal sequence or protease inhibitor domain, was cloned and expressed in *E. coli* with a fused 6x Histidine tag (His tag). Following expression, affinity chromatography facilitated the purification of the protein. For the enzymatic assay, purified PaCP1 underwent incubation with FTC-casein, a casein substrate exhibiting fluorescence upon proteolytic cleavage. Fluorescence intensity was quantified as relative fluorescence units (RFU) which is obtained by subtracting fluorescence measurements of blank controls (FTC-casein substrate incubated with buffer only) from those of experimental samples. As PaCP1 lacked prior characterization, determining its optimal pH for enzymatic activity was imperative. Consequently, PaCP1 and FTC-casein were incubated for 3 hours at room temperature in buffers spanning pH 4 to 7.5, revealing pH 6 as optimal for PaCP1's enzymatic activity (Figure 7A). Based on these results, any subsequent enzymatic assay using purified PaCP1 was performed at pH 6. We then compared PaCP1's activity with that of a known protease, employing papain as a positive control due to PaCP1's classification as a papain-like cysteine protease. Notably, comparable levels of enzymatic activity were observed between PaCP1 and papain following a 3-hour substrate incubation (Figure 7B), thus confirming PaCP1's enzymatic functionality. Further confirmation of PaCP1's classification as a cysteine protease was shown by its incubation with E-64, a known irreversible inhibitor of cysteine proteases, resulting in significantly less substrate cleavage (Figure

7B). To further characterize PaCP1's enzymatic activity, we performed kinetic assays to determine the rate of the enzymatic reaction. Using the Michaelis-Menten equation, we determined the K_m and the V_{max} associated with 0.1 µg of purified PaCP1 (which was the working amount for all previous characterization steps). After incubating purified PaCP1 with FTC-Casein at 22°C for 1 hour, we determined that 0.1 µg of enzyme cleaved the substrate with a K_m of 2.042 µM and a V_{max} of 4545 RFU/µg x mins (Figure 7C). The low value of the K_m indicates a high binding affinity of the enzyme for its substrate. These results not only confirm PaCP1's enzymatic activity and classification as a cysteine protease but also lay a foundation for understanding its functional significance within pokeweed.

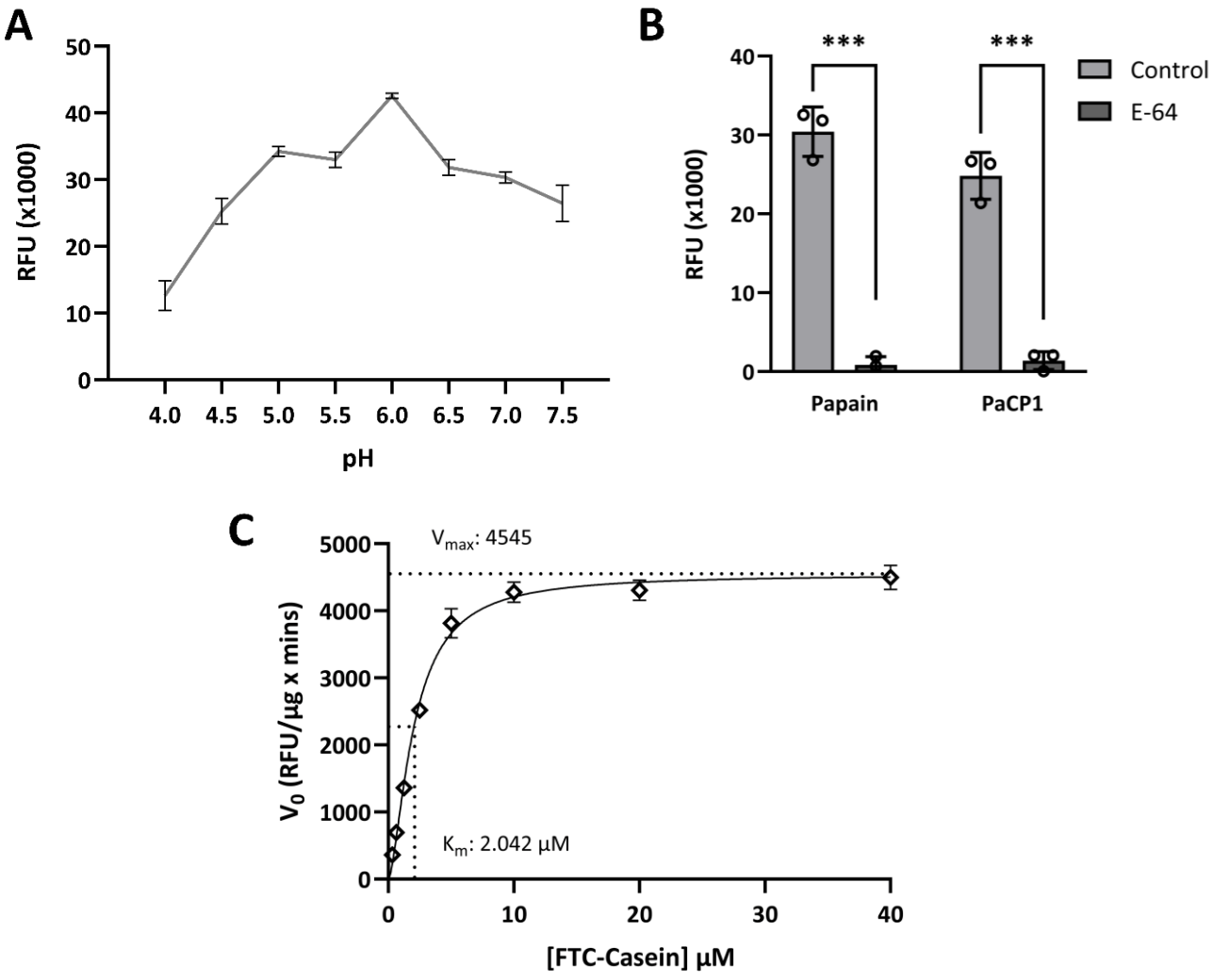

Figure 7. Enzymatic activity of purified PaCP1. (A) Proteolytic activity of purified PaCP1 over a range of pH (4-7.5). RFU of the cleaved fluorescent substrate was measured after a 3-hour incubation with the protease at 22°C. Values are means ± standard deviation of n = 3 independent experiments. Independent experiment results were obtained from three technical replicates. (B) Proteolytic activity of papain and purified PaCP1. Control samples represent an incubation with the fluorescent substrate and papain or PaCP1 only. The E-64 samples are supplemented with 100 μM E-64. Values are means ± standard deviation of n = 3 independent experiments. Independent experiment results were obtained from three technical replicates. p values were calculated by two-tailed unpaired t-test (***, $p < 0.001$). (C) Enzyme kinetics of 0.1 μg of purified PaCP1 at varying FTC-Casein substrate concentrations (0.3 μM to 40.0 μM) after a 1 hour incubation at 22°C.

3.3 Confirming PAP-PaCP1 Protein-Protein Interaction

To validate the initial identification of PaCP1 as a PAP interactor, we conducted a yeast-two hybrid assay using the ProQuest™ Two-Hybrid System (Invitrogen). The mature nucleotide sequence of PaCP1 (comprising the C1A peptidase domain only) and the nucleotide sequence of PAPx (an inactive PAP mutant with a single amino acid mutation in its active site; Hur et al., 1995) were separately cloned into Gateway™ destination vectors pDEST™32 (bait) and pDEST™22 (prey) via gateway cloning. We opted for the PAPx sequence over the native PAP sequence to prevent potential yeast growth issues stemming from rRNA depurination. Subsequently, these plasmids were transformed into the *Saccharomyces cerevisiae* (*S. cerevisiae*; yeast) MaV203 strain. Initial confirmation of successful transformation was achieved by plating yeast on selective media lacking leucine and tryptophan (-Leu/-Trp), yielding positive growth as a transformation control (left panel, Figure 8). The interaction between PaCP1 and PAPx was confirmed by observing yeast growth on selective media lacking leucine, tryptophan, and histidine (-Leu/-Trp/-His), while empty vectors (EV) failed to show growth (right panel, Figure 8). Our experimental setup included control plasmids based on the interaction of Krev1, a member of the Ras family of GTP binding proteins, with RalGDS, the Ral guanine nucleotide dissociator stimulator protein (Benincore-Flórez et al., 2022). Utilizing RalGDS mutants, (RalGDS-m1 and RalGDS-m2 which weaken or abolish the interaction with Krev1 respectively) served as positive and negative controls for the assay. The self-activation controls, PAPx/22 and PaCP1/22, also show no growth on selective media, indicating the absence of self-activation of the reporter gene (*HIS3*) (right panel, Figure 8). Moreover, to explore whether PAP binds to the inactive form of PaCP1 (Pro-PaCP1; comprising the pro inhibitory domain and C1A peptidase domain) or to the mature proteolytically

active protein, we cloned the Pro-PaCP1 nucleotide sequence into pDEST^{TM}22 (prey) and assessed its interaction with PAPx. Notably, no growth of PAPx/Pro-PaCP1 was observed on -Leu/-Trp/-His selective media (right panel, Figure 8). These findings affirm the interaction between PAP and mature PaCP1, corroborating the initial identification made via immunoprecipitation and mass spectrometry techniques.

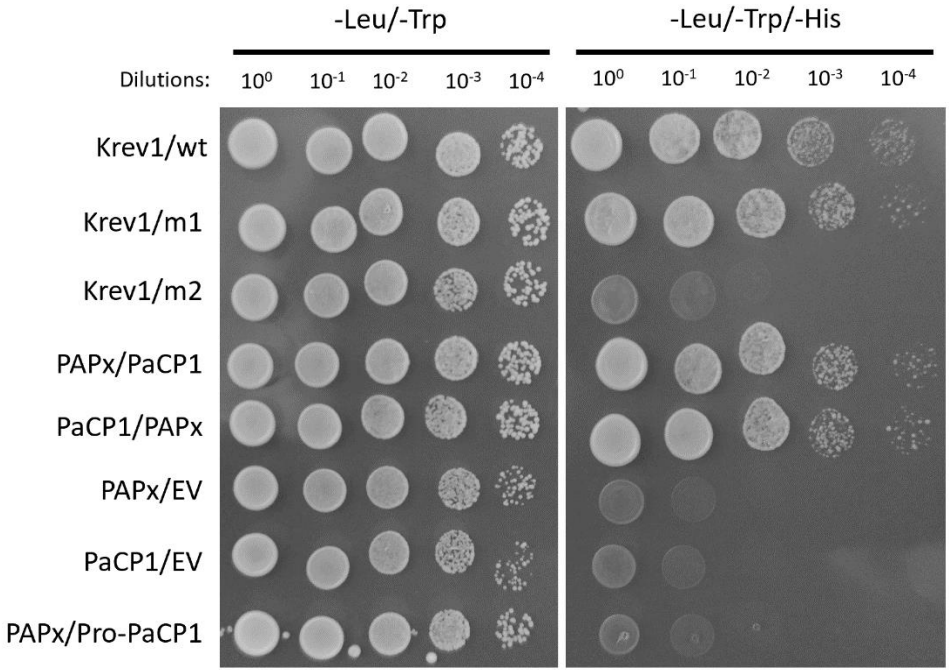

Figure 8. Confirmation of PAP-PaCP1 interaction. Yeast-two hybrid assay testing the interaction between PAPx and PaCP1. Growth of yeast cells on -Leu/-Trp/-His selective media represent positive protein-protein interaction. The same cells are plated on -Leu/-Trp to confirm yeast transformation. Different dilutions of cells are used to test the interaction. Yeast transformed with empty vectors (EV) serve as negative activation control. Pro-PaCP1 is PaCP1 with its pro-inhibitory domain. Krev1/wt: strong positive interaction control. Krev1/m1: weak positive interaction control. Krev1/m2: negative interaction control.

3.4 Co-localization of PAP and PaCP1

From the bioinformatics analysis performed in section 3.1, we know that AtXCP1 localizes in the extracellular space (Chen et al., 2023), implying a potential localization of PaCP1 in the pokeweed apoplast. To support this assumption, the amino acid sequence of PaCP1 was analysed

using DeepLoc 2.0 localization prediction software, which indicated a high probability (0.7699) of extracellular localization (Figure 9A; Thumuluri et al., 2022). This prediction was subsequently confirmed by cloning the full nucleotide sequence of PaCP1 (comprising all domains) into pGWB405, a plant expression vector enabling C-terminal tagging of the protein of interest with eGFP, via Gateway^{TM} cloning. *Nicotiana benthamiana* (*N. benthamiana*) plants were agroinfiltrated with PaCP1-eGFP or empty vector-eGFP (EV-eGFP). Observation of leaf epidermal cells from the PaCP1-eGFP agroinfiltrated plants under a fluorescent microscope revealed the presence of eGFP in the extracellular space upon inducing plasmolysis (Figure 9B). The plants agroinfiltrated with EV-eGFP showed no discernible presence of eGFP in the extracellular space (Figure 9B). RT-PCR analysis employing PaCP1-specific primers validated PaCP1 expression in the PaCP1-eGFP agroinfiltrated *N. benthamiana* leaves but not in EV-eGFP (Figure 9C). Moreover, existing literature and previous research in our lab confirmed the abundance of PAP in the pokeweed extracellular space (Ready et al., 1986). Subsequent validation involved the extraction of apoplastic fluid (AF) from pokeweed plants using the infiltration-centrifugation method (O'Leary et al., 2014). Western blot analysis of the extracted AF, probed with a PAP-specific antibody, distinctly revealed the presence of PAP alongside discernible degradation products (Figure 9D). To detect the presence of papain-like cysteine proteases in AF, we probed the samples with a papain-specific antibody. Since we did not possess a PaCP1-specific antibody, our approach does not definitively confirm the presence of PaCP1 in AF, but it does confirm the presence of papain-like cysteine proteases (Figure 9D). The specificity of the antibody to PaCP1 was validated by the presence of a band in the lane containing purified PaCP1 only (Figure 9D; PaCP1 Std). To ensure that our AF samples were free from cytoplasmic contamination, we also probed the samples with anti-β-actin and anti-ribosomal protein uS3 antibodies. The absence of these cytoplasmic markers in the AF samples confirmed the purity of our AF extraction process (Figure 9D). To verify the presence of all four proteins in pokeweed, total pokeweed lysate was loaded into the far-right lane. These collective findings provide strong evidence supporting the extracellular localization of both PaCP1 and PAP in pokeweed.

A

PaCP1

Predicted localizations: Extracellular

Predicted signals:

Localization	Cytoplasm	Nucleus	Extracellular	Cell membrane	Mitochondrion	Plastid	Endoplasmic reticulum	Lysosome/Vacuole	Golgi apparatus	Peroxisome
Probability	0.4479	0.2423	0.7699	0.3614	0.3072	0.1812	0.1086	0.2180	0.1436	0.0628

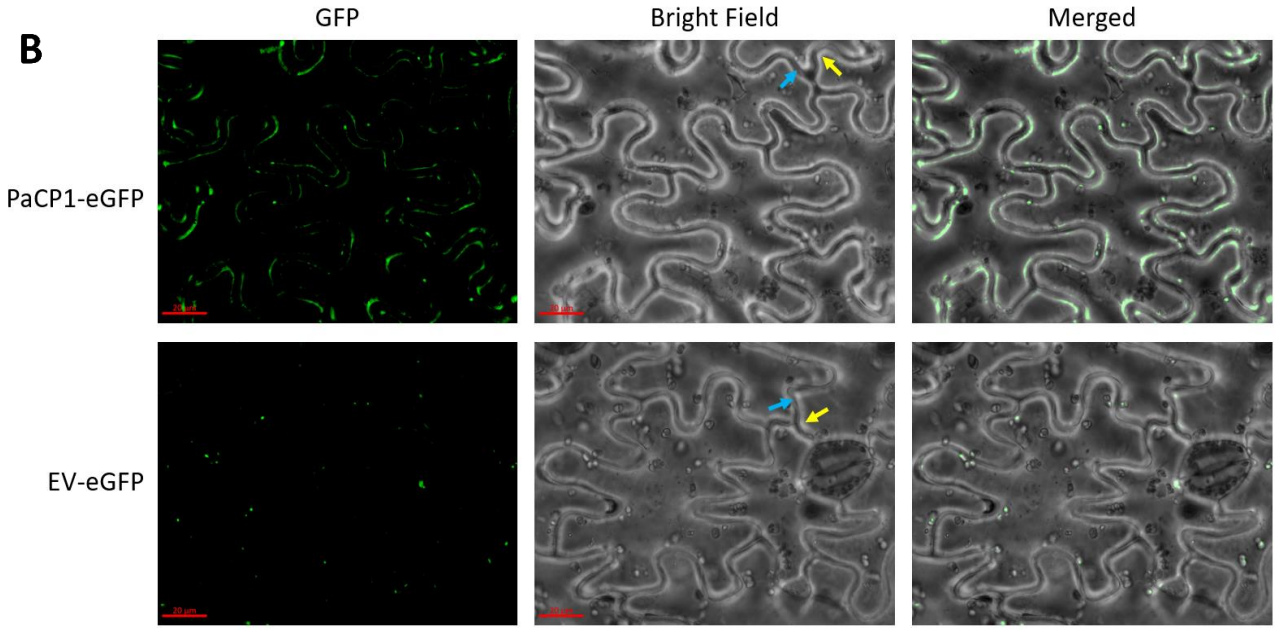

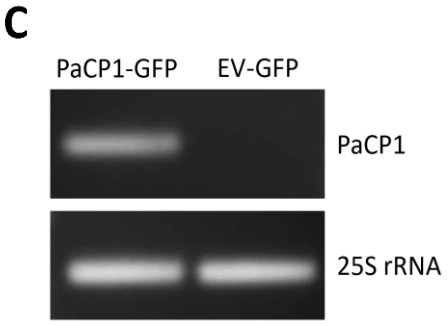

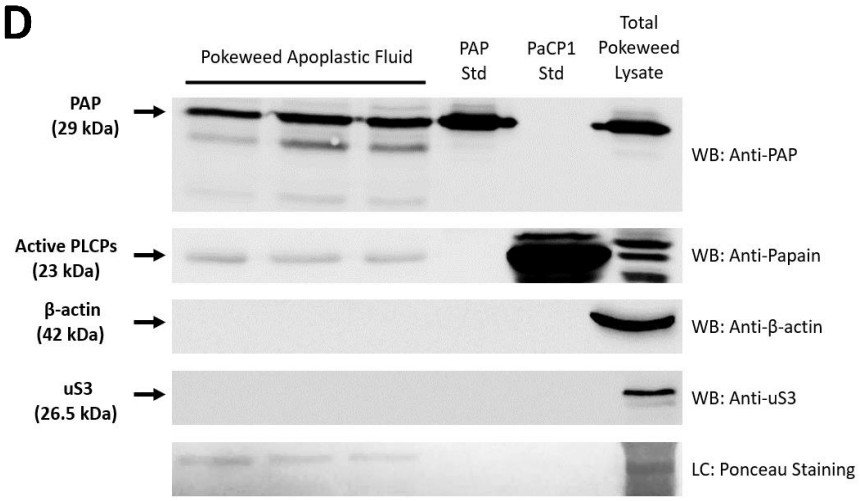

Figure 9. PaCP1 and PAP localization to the extracellular space. (A) Results obtained from DeepLoc 2.0 localization prediction software using PaCP1 amino acid sequence as the input. The probability score of the predicted localization is highlighted in green. (B) Fluorescence microscopy images showing PaCP1-eGFP localized to the extracellular space of *N. benthamiana*, after salt-induced plasmolysis. EV-eGFP serves as a negative control. Scale bars = 20 μM. Blue arrow represents the plant cell wall and the yellow arrow represents the plasma membrane pulling away from the cell wall. (C) RT-PCR using PaCP1 specific primers confirming PaCP1 expression in agroinfiltrated *N. benthamiana*. 25S rRNA served as a positive loading control. (D) Western blot using anti-PAP and anti-papain antibodies confirming presence of PAP and papain-like cysteine protease in apoplastic fluid extracted from pokeweed leaves. WB using anti-β-actin and anti-ribosomal protein uS3 antibodies serve as controls for the absence of cytoplasmic protein contamination. The pokeweed apoplastic fluid represents three samples of independent apoplastic fluid extractions. A PAP and PaCP1 protein standard are loaded to serve as positive and/or negative controls. A sample of total pokeweed proteins is loaded in the far-right lane.

3.5 Biological Significance of PAP-PaCP1 Interaction

A structural prediction of the PAP-PaCP1 interaction was generated using the colab implementation of AlphaFold multimer using default settings (Evans et al., 2021). The prediction model shows the two proteins interacting in a way that covers both of their active sites (Figure 10A). This configuration suggests the potential for the interaction to inhibit the activity of either protein. To assess whether PAP inhibits PaCP1 activity, we conducted an enzymatic cleavage assay (fluorescence assay mentioned section 3.2), incorporating PAP into the reaction mixture. Despite increasing amounts of PAP relative to PaCP1, ranging from 1:1 to 1:100, fluorescence readings showed no significant differences between incubations with or without PAP (Figure 10B). Even when PAP was present in excess, PaCP1 maintained its enzymatic activity, consistent with control conditions. Additionally, considering PaCP1 is an enzymatically active cysteine protease, we explored its potential to proteolytically cleave PAP. Incubating PaCP1 and PAP at a 1:10 ratio for 3 hours, followed by western blot analysis using anti-PAP antibody, revealed bands of lower molecular weight (approximately 24 kDa and 18 kDa) compared to mature PAP (29 kDa), indicative of protein degradation (Figure 10C). Notably, these lower molecular weight bands corresponded to those observed in the apoplastic fluid samples on the PAP western blot in Figure 10D, suggesting that PaCP1 may indeed cleave PAP within the apoplast.

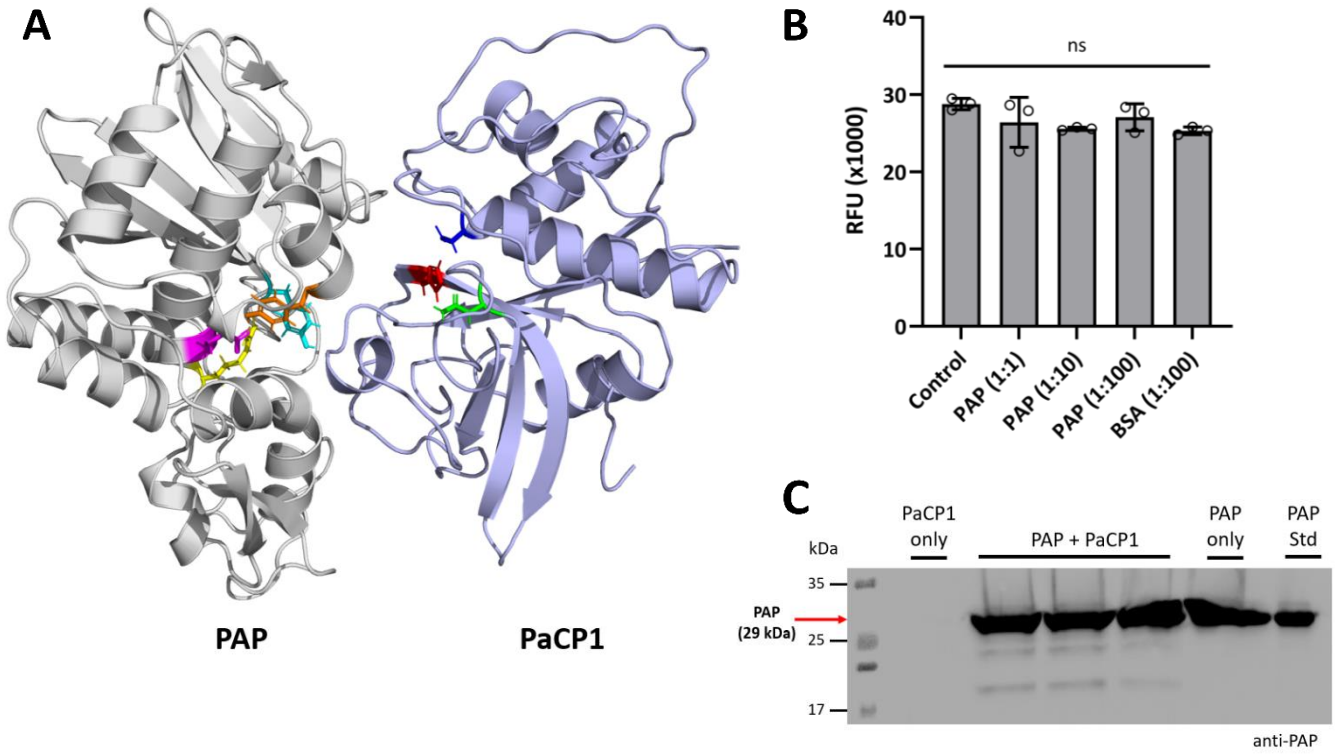

Figure 10. Potential biological significance of PAP-PaCP1 interaction. (A) Structural prediction of the mature PaCP1 (light blue) and PAP (grey) protein-protein interaction using the colab implementation of AlphaFold multimer. The three catalytic residues of the PaCP1 active site are coloured in the same way as presented in Figure 1. The residues of the PAP active site are coloured as follows: tyrosine (Y72) in cyan, tyrosine (Y123) in orange, glutamic acid (E176) in pink, and arginine (R179) in yellow. (B) Enzymatic activity of purified PaCP1 in the presence of increasing amounts of PAP. Control sample represents the fluorescent substrate with PaCP1 only. This was supplemented with PAP in ratios of 1:1, 1:10 and 1:100 (PaCP1: PAP) in subsequent samples. BSA served as a negative control. RFU of the cleaved fluorescent substrate was measured after a 3-hour incubation at 22°C. Values are means ± standard deviation of n = 3 independent experiments. Independent experiment results were obtained from three technical replicates. p values were calculated by two-tailed unpaired t-test (ns = no significant difference). (C) Western blot using anti-PAP polyclonal antibody showing PAP degradation after 3-hour incubation with 0.1 µg purified PaCP1 and 10 µg of PAP at 22°C. PaCP1 only and PAP only are loaded as negative controls. A protein ladder (kDa) is loaded in the left lane and a PAP standard is loaded as a positive control in the far-right lane.

3.6 Mass spectrometry analysis of PAP breakdown products

To determine the specific regions of PAP cleaved by PaCP1, we performed mass spectrometry analysis on the 24 kDa and 18 kDa PAP breakdown products, which were extracted from an SDS-PAGE gel. By aligning the resulting peptides to the mature PAP amino acid sequence, we identified the regions that were absent due to proteolytic cleavage. The peptides identified by mass spectrometry analysis are those shown in blue and green in Figure 11A for the 24 kDa product samples, while the peptides in green only were found in the 18 kDa product samples. Both breakdown products had missing amino acids from the N- and C-termini. Specifically, the 24 kDa product lacked 15 amino acids from the N-terminus and 26 amino acids from the C-terminus. Similarly, the 18 kDa product was missing 67 amino acids from the N-terminus, along with the same 26 amino acids from the C-terminus. Notably, despite these cleavages, the active site of PAP remained intact. To identify which parts of the 3D structure of PAP was missing, we compared the truncated products to the original PAP 3D structure (Figure 11B). The missing amino acids from the 24 kDa breakdown products are coloured in red (N-terminus) and blue (C-terminus) in Figure 11C, whereas the missing amino acids from the 18 kDa breakdown products are coloured in green (N-terminus) and blue (C-terminus) in Figure 11D. The 18 kDa product was missing an alpha helix and two antiparallel beta sheets in addition to a short beta sheet, alpha helix, and unstructured region missing from the 24 kDa product. These results suggest that PaCP1 selectively cleaves specific end regions of PAP, potentially modulating its function while preserving its enzymatic activity.

A

```
VNTIIYNVGSTTISKYATFLNDLRNEAKDPSLKCYGIPMLPNTNTNPKYVLVELQGSNKKTITLMLRRNN
                YATFLNDLRNEAKDPSLK                YVLVELQGSNKK        RNN
                YATFLNDLRNEAK     CYGIPMLPNTNTNPK           KTITLMLRR
                YATFLNDLR                         YVLVELQGSNK TITLMLRR
                         NEAKDPSLKCYGIPMLPNTNTNPK           KTITLMLR NN
                                                            TITLMLR
LYVMGYSDPFETNKCRYHIFNDISGTERQDVETTLCPNANSRVSKNINFDSRYPTLESKAGVKSRSQVQL
LYVMGYSDPFETNK  YHIFNDISGTERQDVETTLCPNANSR   NINFDSRYPTLESKAGVK  SQVQL
              CRYHIFNDISGTER                  NINFDSRYPTLESK    SRSQVQL
                YHIFNDISGTER                  NINFDSR
LYVMGYSDPFETNK              QDVETTLCPNANSR          YPTLESKAGVK
                                                    YPTLESK
GIQILDSNIGKISGVMSFTEKTEAEFLLVAIQMVSEAARFKYIENQVKTNFNRAFNPNPKVLNLQETWGK
GIQILDSNIGK          TEAEFLLVAIQMVSEAARFKYIENQVK     AFNPNPKVLNLQETWGK
GIQILDSNIGK          TEAEFLLVAIQMVSEAAR  YIENQVK     AFNPNPKVLNLQETWGK
           ISGVMSFTEK                    FKYIENQVK     AFNPNPK
                                                              VLNLQETWGK
                                                              VLNLQETWGK
ISTAIHDAKNGVLPKPLELVDASGAKWIVLRVDEIKPDVALLNYVGGSCQTT
ISTAIHDAK      PLELVDASGAK
         NGVLPKPLELVDASGAKWIVLR
ISTAIHDAK
ISTAIHDAK
         NGVLPKPLELVDASGAK
```

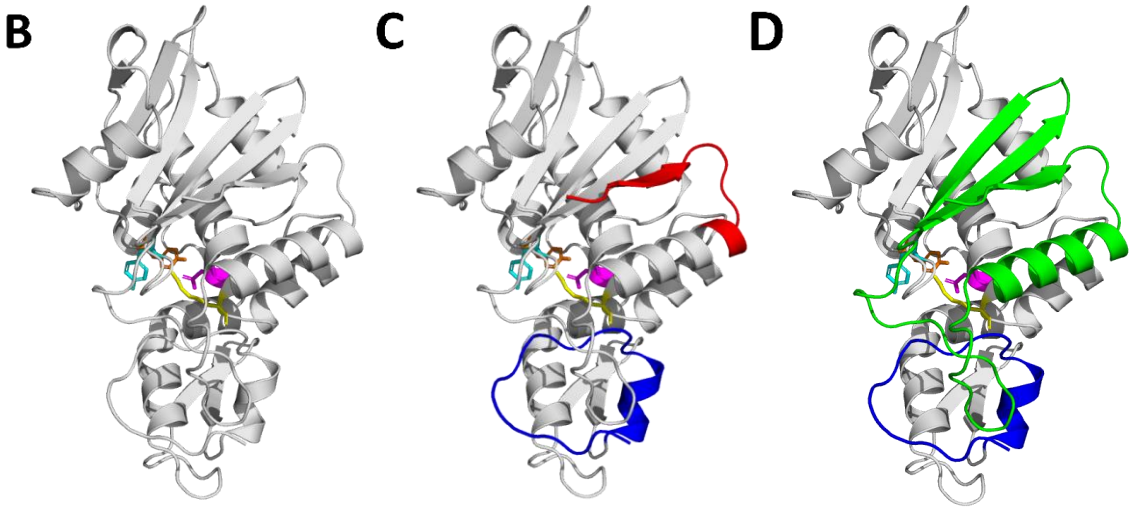

Figure 11. Mass spectrometry analysis of PAP breakdown products. (A) Amino acid alignment of the peptides identified by mass spectrometry for the 24 kDa and 18 kDa PAP breakdown products. The amino acids sequence of mature PAP is highlighted in grey. The amino acids of the PAP active site are coloured as follows: tyrosine (Y72) in cyan, tyrosine (Y123) in orange, glutamic acid (E176) in pink, and arginine (R179) in yellow. The peptides highlighted in blue were found in the 24 kDa product samples only, while the peptides highlighted in green were found in both the 24 and 18 kDa breakdown products. (B) 3D cartoon structure of PAP was obtained from the AlphaFold Protein Structure Database (Jumper et al., 2021; Váradi et al., 2023). The structure of the mature form of PAP is coloured in grey (without the N- and C-terminal sequences). The PAP active site amino acids are coloured the same as in (A). (C) 3D cartoon structure of PAP with the amino acids missing from the 24 kDa breakdown product coloured in red (N-terminus) and in blue (C-terminus). (D) 3D cartoon structure of PAP with the amino acids missing from the 18 kDa breakdown product coloured in green (N-terminus) and in blue (C-terminus).

3.7 Gene expression of PaCP1 and PAP during SA and Flg22 treatment

To assess whether common immunity elicitors would cause transcriptional changes of PaCP1 and PAP, pokeweed plants were subjected to treatment with SA and Flg22. We analysed the isolated RNA from the treated leaves using qPCR to quantify any changes in transcript levels. Our analysis revealed no significant changes in the gene expression of PaCP1 for both treatments, indicating that these elicitors did not influence PaCP1 transcript levels (Figure 12A and 12D). In contrast, the expression of PAP RNA displayed a response to SA, with a notable decrease at 1 and 2 hours post-treatment before returning to normal levels at 4 and 6 hours (Figure 12B). To confirm the efficacy of salicylic acid treatment of pokeweed plants, we monitored the expression of the PR1 gene, a well-established marker of salicylic acid response. PR1 expression remained steady at 1 and 2 hours but showed a significant increase at 4 hours, maintaining this elevated gene expression at 6 hours post treatment (Figure 12C). Additionally, Flg22 treatment induced a significant reduction in PAP RNA levels at 2 and 4 hours, followed by an increase at 6 hours (Figure 12E). Therefore, the transcript levels of each gene responded differently to these elicitors of stress.

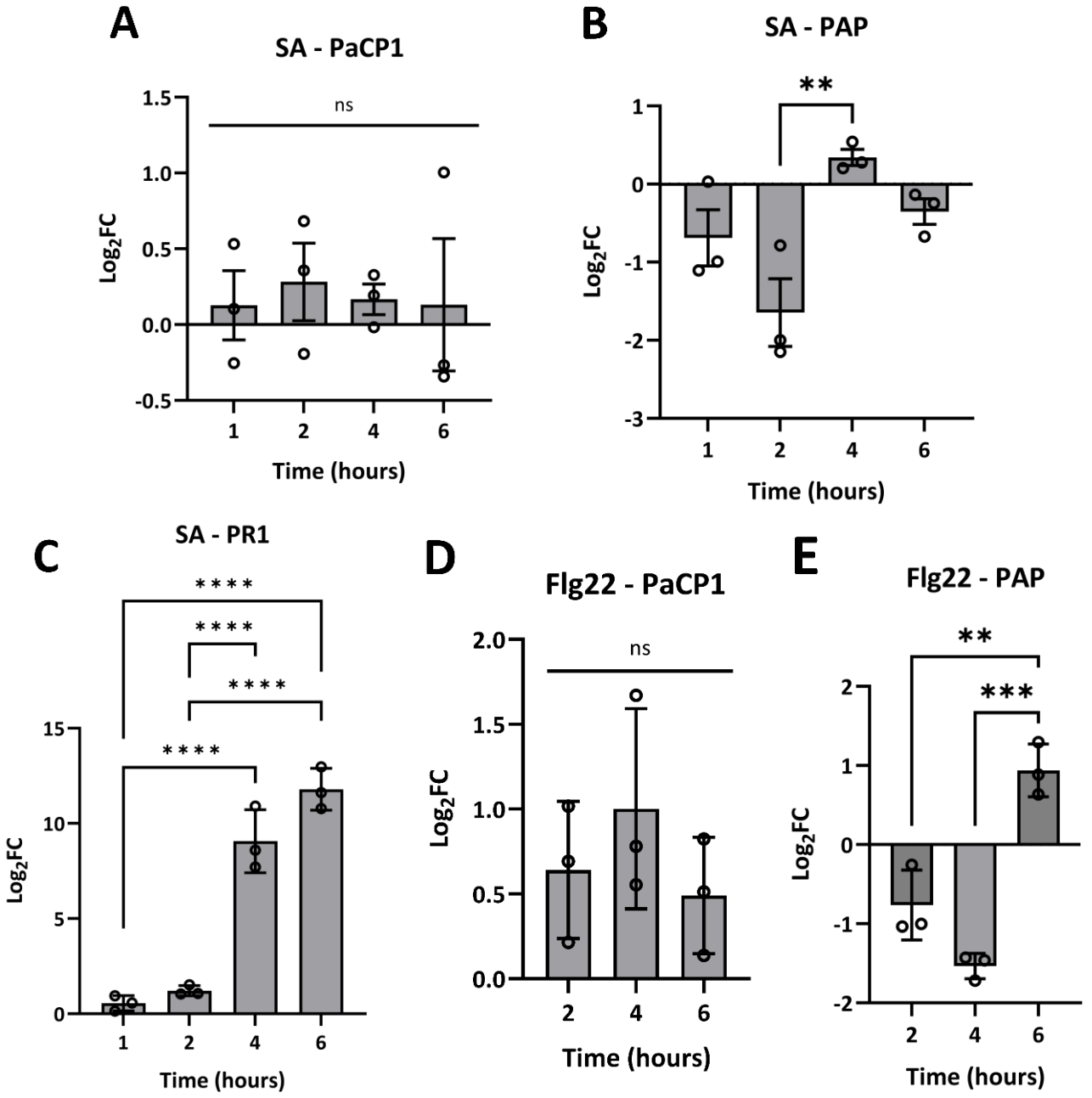

Figure 12. PAP and PaCP1 gene expression by qRT-PCR analysis during SA and Flg22 treatment of pokeweed plants. (A) PaCP1 transcript levels (Log_2FC) after 1, 2, 4, and 6 hours post-treatment with SA. (B) PaCP1 transcript levels (Log_2FC) after 1, 2, 4, and 6 hours post-treatment with SA. (C) PR1 transcript levels (Log_2FC) after 1, 2, 4, and 6 hours post-treatment with SA. (D) PaCP1 transcript levels (Log_2FC) after 2, 4, and 6 hours post-treatment with Flg22. (E) PAP transcript levels (Log_2FC) after 2, 4, and 6 hours post-treatment with Flg22. Log_2FC = Log_2 fold change. Poly-A binding protein and dynamin served as reference genes for normalization. Values are means ± standard deviation of n = 3 independent experiments. Error bars represent the standard deviation. p values were calculated by a one-way ANOVA test, ns = no significant difference, ** = $p < 0.001$, *** = $p < 0.001$, **** = $p < 0.0001$.

4. DISCUSSION

4.1 Summary of main findings

This study focused on characterising a novel cysteine protease from pokeweed, identified as *Phytolacca americana* cysteine protease 1 (PaCP1), and investigating its interaction with PAP. Through bioinformatics analysis, PaCP1 was predicted to be a papain-like cysteine protease with an extracellular localization. Enzymatic activity assays confirmed its proteolytic activity, showing optimal activity at pH 6 and inhibition by the cysteine protease inhibitor E-64. Kinetic analysis revealed a high binding affinity for its substrate, further corroborating its classification as a functional cysteine protease. Moreover, a yeast two-hybrid assay demonstrated a specific interaction between mature PaCP1 and PAPx, with no interaction observed with the inactive precursor form of PaCP1. This interaction was further supported by co-localization studies in *N. benthamiana*, where PaCP1 was found in the extracellular space and PAP was present in apoplastic fluid samples. Interestingly, we discovered the presence of PAP degradation products in pokeweed apoplastic fluid. Furthermore, mass spectrometry analysis of these degradation products identified specific cleavage sites, showing that PaCP1 cleaves PAP at both the N- and C-termini. Additionally, qPCR analysis revealed differential expression patterns of PaCP1 and PAP in response to SA and Flg22 treatments. While PaCP1 transcript levels remained unchanged, PAP showed a transient decrease in response to SA and a fluctuating pattern with Flg22, indicating complex regulation under stress conditions. Together, these findings provide new insights into the functional roles of PaCP1 and PAP in pokeweed, suggesting a potential mechanism of immune modulation through proteolytic processing. This study lays the groundwork for further exploration of the biological significance of PAP cleavage by PaCP1 and its implications for plant defence strategies.

4.2 Comparison of PaCP1 to other papain-like cysteine proteases

PaCP1, identified as a member of the papain-like cysteine protease (PLCP) family, exhibits characteristics typical of this group, including a conserved catalytic triad of amino acids (C156, H291, N311) (Misas-Villamil et al., 2016). Similar to other PLCPs, PaCP1 is synthesised as an inactive precursor containing a signal peptide and a protease inhibitor domain, which undergoes proteolytic processing to become active. The apoplastic localization of PaCP1 implies a potential role in plant immunity, as the apoplast is the first barrier encountered by pathogens during invasion

(Farvardin et al., 2020). Understanding the function and potential substrates of PLCPs is crucial for elucidating the plant immune response. However, determining the potential substrates of plant proteases is challenging due to the lack of common recognition motifs (Turk et al., 2012; Fernández-Fernández et al., 2023). Additionally, identifying the regulatory mechanisms that control plant protease activity remains an ongoing area of research (Fernández-Fernández et al., 2023).

In Arabidopsis, AtXCP1 has been shown to cleave the propeptide of pathogenesis-related protein 1 (AtPR1) and proteolytically activates AtCAPE9 (Chen et al., 2023). The release of AtCAPE9 from PR1 induces the accumulation of SA in Arabidopsis leaves. Increased SA levels and infection by *Pseudomonas syringae* subsequently enhance the proteolytic activity of AtXCP1, creating a positive feedback loop (Chen et al., 2023). This study also identified pH 6 as the optimal pH for AtXCP1 enzymatic activity (AtXCP1 is the protein with the highest homology to PaCP1), which is consistent with our enzymatic assay results for PaCP1 (Chen et al., 2023). As previously mentioned, the pH of the apoplast ranges from 4.5 to 5.5 (Geilfus et al., 2020a,b) and several studies have shown alkalinization upon exposure to a variety of abiotic and biotic stresses (Felle, 2001; Felle et al., 2004; Felle et al., 2009; Geilfus, 2017). The optimal pH for PaCP1 is slightly higher than the pH of the apoplast. However, if the pokeweed apoplast also undergoes alkalinization during exposure to stress, this would suggest a role for PaCP1 enzymatic activity in the plant's stress response.

In maize, apoplastic PLCPs are responsible for the cleavage of Zip1 from its propeptide precursor ProZip1 (Ziemann et al., 2018; Wang et al., 2020; Godson & van der Hoorn, 2021). The Zip1 peptide acts as a damage-associated molecular pattern (DAMP) and is involved in immune signalling. Similar to AtCAPE9, Zip1 enhances SA accumulation, which in turn induces PLCP activity, forming a positive feedback loop (Ziemann et al., 2018; Godson & van der Hoorn, 2021). The release of Zip1 also upregulates defence genes in maize. Although the specific PLCP responsible for ProZip1 cleavage has not been identified, the authors suggested that multiple apoplastic PLCPs may be involved (Ziemann et al., 2018).

A recent study has highlighted the role of an apoplastic PLCP in antiviral defence and immunity, an area that has been largely unexplored. Liu et al. (2023) demonstrated that the apoplastic PLCP TaRD21A from wheat plays a crucial role in conferring resistance to wheat yellow

mosaic virus (WYMV). The study revealed that TaRD21A's proteolytic activity releases a small signal peptide, Wip1, from its precursor protein PROWIP1. This peptide significantly reduced WYMV infection and viral RNA levels when applied to wheat, underscoring its potential as an antiviral agent. The study concluded that TaRD21A's contribution to wheat resistance against WYMV relies on its catalytic function, which generates the immune-facilitating Wip1 peptide (Liu et al., 2023).

These findings emphasise the role of PLCPs in generating small peptides that enhance plant immunity. Many apoplastic PLCPs contribute to plant defence through their proteolytic activity, which involves cleaving proteins to release signalling peptides (Misas-Villamil et al., 2016). Our research indicates that PaCP1, localised in the apoplast, not only exhibits proteolytic activity but also cleaves PAP, releasing truncated protein products and small peptides. This suggests a role for PaCP1 immune signalling and underscores its potential importance in the broader context of plant immunity.

4.3 Known protein interactions of papain-like cysteine protease

Most of the documented interactions involving papain-like cysteine proteases (PLCPs) are with inhibitors, either endogenous or pathogen-derived. These inhibitors play critical roles in modulating protease activity and, consequently, plant immunity. Plant cystatins are a primary group of endogenous inhibitors that target PLCPs, effectively regulating their activity (Martinez et al., 2009; van der Linde et al., 2012). In maize (*Zea mays*), the biotrophic fungus *Ustilago maydis* manipulates the host plant's immune response by inducing the expression of a cysteine protease inhibitor, CC9, during early infection. The production of maize cysteine proteases is upregulated upon *U. maydis* infection, but simultaneously, the fungus induces the production of CC9 to inhibit these proteases, thereby aiding its pathogenicity (van der Linde et al., 2012a,b; Mueller et al., 2013; Jashni et al., 2015). Furthermore, in Arabidopsis the protein Pirin2 (PRN2) interacts with XCP2, a PLCP similar to AtXCP1, inhibiting its activity (Zhang et al., 2014). PRN2 stabilises XCP2 and prevents its autocatalytic degradation, despite lacking known protease inhibitor domains like those in cystatins (Zhang et al., 2014). This interaction highlights a novel mechanism of protease inhibition in plants.

In addition to plant cystatins, various pathogens secrete effector proteins that inhibit PLCPs to facilitate infection (Martínez et al., 2012; Misas-Villamil et al., 2016). Numerous examples exist

of different effector proteins from a variety of pathogens targeting diverse PLCPs involved in the immune response. These interactions often lead to the suppression of the plant's immune response, increasing its susceptibility to infections. For example, AtXCP1 in Arabidopsis is targeted by SSPbP53, an apoplastic cystatin-like protein secreted by the parasitic protist *Plasmodiphora brassicae*. SSPbP53 binds and inhibits XCP1's enzymatic activity (Pérez-López et al., 2021). Additionally, downregulation of AtXCP1 expression is observed in infected Arabidopsis roots compared to mock-inoculated controls, underscoring the pathogen's strategy to suppress host immune responses (Pérez-López et al., 2021). Moreover, in tomato, the Avr2 effector from *Cladosporium fulvum* binds to the apoplastic cysteine protease Rcr3, which is essential for plant immunity. Avr2 directly inhibits Rcr3's protease activity, promoting infection by *C. fulvum* (Shabab et al., 2008; van Esse et al., 2008; Wang et al., 2020). This interaction exemplifies how pathogen effectors can manipulate host protease activity to evade immune responses. Another example is the interaction between the sugarcane mosaic virus (SCMV) and maize. SCMV enhances the activation of Corn Cysteine Protease 1 (CCP1) and induces the SA signalling pathway in maize (Yuan et al., 2024). However, the SCMV-encoded NIa-Pro protein interacts with CCP1 to inhibit its activity, undermining maize's resistance to SCMV (Yuan et al., 2024). This highlights the role of PLCPs in plant defence against a wide range of microbial pathogens, including bacteria, fungi, and viruses.

These interactions underscore the complexity of PLCP regulation and its crucial role in plant immunity. While our results show that PAP does not inhibit PaCP1 activity (Figure 10B), it is clear that the interaction between these two proteins must serve a different purpose. PAP does not act as an endogenous inhibitor of PaCP1, but this does not preclude PAP from inhibiting other apoplastic proteins or PaCP1 being inhibited by other molecules or proteins, such as cystatins. Understanding these interactions can provide deeper insights into the regulatory mechanisms governing pokeweed immune responses.

4.4 Interaction of PAP and PaCP1

In the context of pokeweed, PaCP1's interaction with PAP does not inhibit PaCP1’s enzymatic activity (as shown in Figure 10B); however, the interaction could be part of a broader mechanism regulating PAP's depurination activity. Considering that PAP is known to inhibit translation elongation, the interaction with PaCP1 might modulate PAP's activity or stability,

thereby influencing its enzymatic activity. PAP has been well-documented to interact with the L3 ribosomal protein, and translation initiation factor eIFiso4G (Hudak et al., 1999; Wang & Hudak, 2006). These interactions underline PAP's primary function as a ribosome-inactivating protein (RIP), which cleaves the N-glycosidic bond of adenine residues in rRNA, thus inhibiting protein synthesis (Ready et al., 1986).

The identification of PAP-PaCP1 interaction in the apoplast, however, introduces a novel aspect of PAP's function within the extracellular space. The apoplast is a critical site for plant-pathogen interactions and immune responses. The presence of PAP in the apoplast and its interaction with PaCP1 suggest a potential role in the extracellular defence mechanisms of pokeweed. This novel interaction may influence how PAP contributes to pokeweed's overall immune strategy, possibly by interacting with other apoplastic proteins involved in defence or acting as an RNA binding protein protecting extracellular RNAs (Gnanasekaran & Moffett, 2015; Lee et al., 2010; Karimi et al., 2022).

Notably, the interaction between PAP and PaCP1 might suggest a mechanism where PAP’s activity is regulated in the apoplast. Given that the two proteins do not interact when PaCP1 is in its inactive form (Figure 8), this further supports the idea that PaCP1 interacts with PAP primarily to cleave it and that this interaction would not likely exist until each protein reached the apoplast. This proteolytic regulation aligns with the broader role of cysteine proteases in modulating the function of key proteins involved in plant defence (van der Hoorn & Kamoun, 2008; Delauré et al., 2008). The cleavage of PAP by PaCP1 might alter its activity or stability, potentially generating peptide fragments with distinct functions.

4.5 Role of PAP cleavage by PaCP1

Though the crystal structure of PAP has been determined (Monzingo et al., 1993; Zeng et al., 2003), the importance of specific structural regions of PAP remains underexplored. The cleavage of PAP by PaCP1 could potentially regulate PAP’s depurination activity by altering its structure and function. In plant immunity, proteolytic processing by cysteine proteases often modulates the activity of defence-related proteins, either activating or deactivating thereby adjusting the immune response (van der Hoorn & Kamoun, 2008; Delauré et al., 2008).

PaCP1's cleavage of PAP may possibly convert PAP into a form with altered activity against pathogens. Notably, previous studies have demonstrated that the deletion of the first 16 amino

acids of the mature PAP N-terminus eliminated its cytotoxicity and ribosomal depurination activity in yeast (Hudak et al., 2004). Based on our results, the 24 kDa PAP breakdown product lacks the first 15 amino acids, indicating a potential loss of depurination activity. The 18 kDa product is missing 67 amino acids from the N-terminus, suggesting an even higher likelihood of losing depurination activity against ribosomes. Similarly, the same study shows that deletion of the last 19 amino acids of the mature PAP C-terminus abolishes its cytotoxicity and ribosomal depurination activity in yeast (Hudak et al., 2004). Given that both the 24 and 18 kDa PAP breakdown products identified in our study are missing the last 26 amino acids, it is likely that neither of these products retain depurination activity against ribosomes.

Considering that this cleavage likely occurs in the extracellular space, where intact ribosomes are absent, the loss of rRNA depurination activity may not be critical. However, this does not exclude the possibility that the breakdown products could still depurinate RNA molecules due to differences in their structural configurations. Alternatively, the 24 and 18 kDa PAP products may have lost all enzymatic activity. Despite PaCP1's cleavage of PAP, it does not completely eliminate wild-type mature PAP, as significant amounts of intact PAP remain in the apoplastic fluid samples (Figure 9D). This suggests that the breakdown products may have additional functions beyond merely being degradation products of PAP. A potential role for the PAP breakdown products could be to act as RNA binding proteins to protect extracellular RNAs. Recent studies have shown the presence of extracellular RNAs outside of vesicles in the Arabidopsis apoplast (Karimi et al., 2022). If those PAP breakdown products have lost their depurination capabilities due to the cleavages of the N- and C-termini, they could act as RNA binding proteins protecting extracellular RNAs from apoplastic nucleases.

Another potential role for the PAP breakdown products is the release of the small peptides from the N- and C-termini. These small peptides, generated by cleaving 15 amino acids from the N-terminus and 26 amino acids from the C-terminus of PAP, could be acting as damage-associated molecular patterns (DAMPs). DAMPs, unlike pathogen-associated molecular patterns (PAMPs), are derived from endogenous host cells and are typically released during pathogen invasion, serving as signals to trigger immune responses (Hou et al., 2019). These small peptides could function similarly to CAPE9, derived from PR1 in Arabidopsis, or Zip1 from maize, both of which are known DAMPs (Chen et al., 2023; Ziemann et al., 2018). Since most identified and studied

DAMPs are apoplastic peptides or extracellular components (Hou et al., 2019), the PAP breakdown products could serve as DAMPs in pokeweed, contributing to the plant's immune response. This would explain why only a portion of the extracellular PAP is cleaved, suggesting a regulated process aimed at maintaining immune signalling rather than simply deactivating PAP.

4.6 Significance of PAP and PaCP1 gene expression during SA and Flg22 treatment

The qPCR analysis conducted in this study provided valuable insights into the transcriptional dynamics of PaCP1 and PAP in pokeweed under treatment with SA and Flg22, both known elicitors of plant immunity (Meena et al., 2022). The results revealed that while PaCP1 transcript levels remained relatively stable, PAP exhibited a distinct pattern of expression in response to these treatments, suggesting differential regulatory mechanisms for PAP and PaCP1. The stable expression of PaCP1 may reflect its role in maintaining basal proteolytic activity in the apoplast, ensuring a ready state for defence activation.

PAP showed a transient decrease in expression upon SA treatment, reaching its lowest level at 2 hours post-treatment before gradually returning to baseline (Figure 12B). This transient suppression could indicate a rapid modulation of PAP levels as part of a regulated immune response, potentially to prevent excessive cytotoxicity during early stages of pathogen attack. The antagonistic nature of SA and JA could also explain this decrease in expression, as PAP is known to be upregulated by JA (Neller et al., 2016; Dougherty et al., 2024). In Arabidopsis, SA treatment downregulates the expression of JA responsive genes (Tamaoki et al., 2013; Yang et al., 2015; Wang et al., 2021). In the case of pokeweed, treatment with SA can cause PAP transcript levels to decrease due to an inhibition of JA-responsive genes by the increased levels of SA.

In contrast, Flg22 treatment elicited a more complex response in PAP expression, characterised by an initial decline at 2 hours, further decline at 4 hours, and subsequent upregulation at 6 hours (Figure 12E). This pattern suggests that PAP may not be involved in the early recognition of PAMPs and that its expression is tightly regulated to balance defence and potential self-damage. However, PAP is highly expressed in leaves as it has been reported that 0.5% of total soluble protein in pokeweed leaves is PAP (Bonness et al., 1994). Therefore, a downregulation at 2 and 4 hours post treatment with Flg22 may not have such a significant influence on the levels of PAP protein.

The stability of PaCP1 transcript levels in response to both treatments is intriguing and suggests that its regulation may occur post-transcriptionally or that its expression is constitutively maintained to provide a ready supply of protease for immediate defence needs. Constitutive expression of cysteine proteases involved in plant defence has been reported in other species. For instance, the PLCP RD21 in Arabidopsis is expressed at a constant level and regulated primarily through post-translational modifications and activation (Yamada et al., 2001). There are some examples, although very few, of other stresses inducing transcript levels of PLCPs. One example is a gene expression analysis in barley that has shown upregulation of PLCPs during leaf senescence, a form of plant cell death (Díaz-Mendoza et al., 2014; Misas-Villamil et al., 2016). Additionally, the Rcr3 PLCP from tomato is upregulated upon pathogen infection (Kruger, 2002; van der Hoorn, 2008). Finally, a recent study has shown that CCP1 from maize is upregulated upon infection with sugarcane mosaic virus (Yuan et al., 2024). This indicates that while SA and Flg22 may not alter PaCP1 transcript levels, other treatments could have different effects.

Although few studies have reported changes in PLCP transcript levels upon stress, many have shown an increase in proteolytic activity. For example, SA treatment activates PLCPs in maize but does not directly affect gene expression (van der Linde et al., 2012a,b; Misas-Villamil et al., 2016). Another study showed increased activity of multiple apoplastic PLCPs in tomato upon infection by *Ralstonia solanacearum* (Planas-Marquès et al., 2018; Godson & van der Hoorn, 2021). This suggests that while the transcript levels of PaCP1 may not increase upon treatment with SA or Flg22, its enzymatic activity could still be enhanced to perform its necessary functions under these stress conditions.

Furthermore, the differential expression patterns of PAP and PaCP1 highlight the complexity of their roles in the pokeweed immune system. While PAP's fluctuating levels suggest a responsive mechanism to specific stress signals, PaCP1's steady expression implies a fundamental role in maintaining homeostasis or readiness for pathogen encounter. In summary, the qPCR results underscore the nuanced regulation of PaCP1 and PAP in pokeweed, reflecting their distinct but complementary roles in plant immunity.

4.7 Future directions

Building on the findings of this study, several avenues for future research are suggested to further elucidate the roles of PaCP1 and PAP in pokeweed immunity. First, investigating the post-

transcriptional mechanisms that regulate PaCP1 activity is crucial. Determining the specific environmental cues or stress conditions that trigger the removal of the pro-domain from PaCP1 and activate its proteolytic function will enhance our understanding of its regulation. Additionally, exploring different stress conditions, such as pathogen infection, drought, or other abiotic stresses, could reveal circumstances under which PaCP1 transcript levels are upregulated, providing insights into its role in plant stress responses.

With the recent sequencing of the pokeweed genome (Dougherty et al., 2024), we can now utilise bioinformatic tools to identify potential cystatins that may inhibit PaCP1. Homology-based searches could uncover candidate cystatins, which could then be experimentally tested for their ability to interact with and inhibit PaCP1. This would shed light on the regulatory networks controlling PaCP1 activity and their implications for plant immunity. Further investigation is needed to determine whether SA or Flg22 treatments increase the proteolytic activity of PaCP1. Understanding if PaCP1 becomes more enzymatically active under these stress conditions will help clarify its role in the immune response. Additionally, examining the extent of PAP degradation in the apoplastic fluid following various stress treatments, including SA, Flg22, and JA, could provide valuable insights into how stress conditions influence the interaction and processing of PAP by PaCP1.

Exploring the potential depurination activity of the PAP breakdown products is another critical area of future research. It will be important to determine whether these truncated forms of PAP can depurinate ribosomes or mRNAs effectively or if they have lost this activity entirely. Such investigations will clarify the functional consequences of PAP cleavage and its impact on plant physiology and immune responses. Furthermore, the possibility that the small peptides released from the cleavage of PAP by PaCP1 act as damage-associated molecular patterns (DAMPs) warrants investigation. These peptides could play significant roles in immune signalling, similar to other known DAMPs in plants. Experimental approaches could involve treating plants with synthetic peptides corresponding to the cleaved fragments and assessing their effects on immune gene expression and overall plant defence responses.

Finally, conducting co-immunoprecipitation and mass spectrometry analyses to identify additional interacting partners of PaCP1 and PAP in the apoplast could reveal new components of the pokeweed immune system. Understanding these interactions will provide a more

comprehensive picture of the complex regulatory networks and defence mechanisms in which PaCP1 and PAP are involved.

Overall, these future research directions aim to deepen our understanding of the functional roles and regulatory mechanisms of PaCP1 and PAP in pokeweed, contributing to the broader knowledge of plant immunity and protease-mediated regulation of defence responses.

5. REFERENCES

Alekseenko, A., Barrett, D., Pareja-Sanchez, Y., Howard, R. J., Strandback, E., Ampah-Korsah, H., Rovšnik, U., Zuniga-Veliz, S., Klenov, A., Malloo, J., Ye, S., Liu, X., Reinius, B., Elsässer, S. J., Nyman, T., Sandh, G., Yin, X., & Pelechano, V. (2021). Direct detection of SARS-CoV-2 using non-commercial RT-LAMP reagents on heat-inactivated samples. *Scientific Reports*, *11*(1). https://doi.org/10.1038/s41598-020-80352-8

Almagro Armenteros, J. J., Salvatore, M., Emanuelsson, O., Winther, O., von Heijne, G., Elofsson, A., & Nielsen, H. (2019). Detecting sequence signals in targeting peptides using deep learning. *Life Science Alliance*, *2*(5), e201900429. https://doi.org/10.26508/lsa.201900429

Aron, G. M., & Irvin, J. D. (1980). Inhibition of herpes simplex virus multiplication by the pokeweed antiviral protein. *Antimicrobial Agents and Chemotherapy*, *17*(6), 1032–1033. https://doi.org/10.1128/aac.17.6.1032

Asai, T., Tena, G., Plotnikova, J., Willmann, M. R., Chiu, W.-L., Gomez-Gomez, L., Boller, T., Ausubel, F. M., & Sheen, J. (2002). MAP kinase signalling cascade in Arabidopsis innate immunity. *Nature*, *415*(6875), 977–983. https://doi.org/10.1038/415977a

Barbieri, L. (1997). Polynucleotide: adenosine glycosidase activity of ribosome-inactivating proteins: effect on DNA, RNA and poly(A). *Nucleic Acids Research*, *25*(3), 518–522. https://doi.org/10.1093/nar/25.3.518

Barbieri, L., Battelli, M. G., & Stirpe, F. (1993). Ribosome-inactivating proteins from plants. *Biochimica et Biophysica Acta (BBA) - Reviews on Biomembranes*, *1154*(3-4), 237–282. https://doi.org/10.1016/0304-4157(93)90002-6

Bateman, A., Martin, M.-J., Orchard, S., Magrane, M., Agivetova, R., Ahmad, S., Alpi, E., Bowler-Barnett, E. H., Britto, R., Bursteinas, B., Bye-A-Jee, H., Coetzee, R., Cukura, A., Da Silva, A., Denny, P., Dogan, T., Ebenezer, T., Fan, J., Castro, L. G., & Garmiri, P. (2020). UniProt: the universal protein knowledgebase in 2021. *Nucleic Acids Research*, *49*(D1), D480–D489. https://doi.org/10.1093/nar/gkaa1100

Benincore-Flórez, E., El-Azaz, J., Solarte, G. A., Rodríguez, A., Reyes, L. H., Alméciga-Díaz, C. J., & Cardona-Ramírez, C. (2022). Iduronate-2-sulfatase interactome: validation by yeast two-hybrid assay. *Heliyon*, *8*(3), e09031. https://doi.org/10.1016/j.heliyon.2022.e09031

Bigeard, J., Colcombet, J., & Hirt, H. (2015). Signaling mechanisms in pattern-triggered immunity (PTI). *Molecular Plant*, *8*(4), 521–539. https://doi.org/10.1016/j.molp.2014.12.022

Boller, T., & Felix, G. (2009). A Renaissance of Elicitors: Perception of Microbe-Associated Molecular Patterns and Danger Signals by Pattern-Recognition Receptors. *Annual Review of Plant Biology*, *60*(1), 379–406. https://doi.org/10.1146/annurev.arplant.57.032905.105346

Bonness, M. S., Ready, M. P., Irvin, J. D., & Mabry, T. J. (1994). Pokeweed antiviral protein inactivates pokeweed ribosomes; implications for the antiviral mechanism. *The Plant Journal*, *5*(2), 173–183. https://doi.org/10.1046/j.1365-313x.1994.05020173.x

Chen, L.-Q., Hou, B.-H., Lalonde, S., Takanaga, H., Hartung, M. L., Qu, X.-Q., Guo, W.-J., Kim, J.-G., Underwood, W., Chaudhuri, B., Chermak, D., Antony, G., White, F. F., Somerville, S. C., Mudgett, M. B., & Frommer, W. B. (2010). Sugar transporters for intercellular exchange and nutrition of pathogens. *Nature*, *468*(7323), 527–532. https://doi.org/10.1038/nature09606

Chen, Y.-L., Lin, F.-W., Cheng, K.-T., Chang, C.-H., Hung, S.-C., Efferth, T., & Chen, Y.-R. (2023). XCP1 cleaves Pathogenesis-related protein 1 into CAPE9 for systemic immunity in Arabidopsis. *Nature Communications*, *14*(1). https://doi.org/10.1038/s41467-023-40406-7

Chen, Z., Antoniw, J. F., & White, R. F. (1993). A possible mechanism for the antiviral activity of pokeweed antiviral protein. *Physiological and Molecular Plant Pathology*, *42*(4), 249–258. https://doi.org/10.1006/pmpp.1993.1023

Chinchilla, D., Zipfel, C., Robatzek, S., Kemmerling, B., Nürnberger, T., Jones, J. D. G., Felix, G., & Boller, T. (2007). A flagellin-induced complex of the receptor FLS2 and BAK1 initiates plant defence. *Nature*, *448*(7152), 497–500. https://doi.org/10.1038/nature05999

Chuang, W.-P., Herde, M., Ray, S., Castano-Duque, L., Howe, G. A., & Luthe, D. S. (2013). Caterpillar attack triggers accumulation of the toxic maize protein RIP2. *New Phytologist*, *201*(3), 928–939. https://doi.org/10.1111/nph.12581

Citores, L., Iglesias, R., & Ferreras, J. M. (2021). Antiviral Activity of Ribosome-Inactivating Proteins. *Toxins*, *13*(2), 80. https://doi.org/10.3390/toxins13020080

Cosgrove, D. J. (2015). Plant cell wall extensibility: connecting plant cell growth with cell wall structure, mechanics, and the action of wall-modifying enzymes. *Journal of Experimental Botany*, *67*(2), 463–476. https://doi.org/10.1093/jxb/erv511

Cosgrove, D. J. (2018). Diffuse Growth of Plant Cell Walls. *Plant Physiology*, *176*(1), 16–27. https://doi.org/10.1104/pp.17.01541

Darino, M., Kanyuka, K., & Hammond-Kosack, Kim E. (2022). Apoplastic and vascular defences. *Essays in Biochemistry*, *66*(5), 595–605. https://doi.org/10.1042/ebc20220159

Delaunois, B., Colby, T. V., Belloy, N., Conreux, A., Harzen, A., Baillieul, F., Clément, C., Schmidt, J., Jeandet, P., & Cordelier, S. (2013). Large-scale proteomic analysis of the grapevine leaf apoplastic fluid reveals mainly stress-related proteins and cell wall modifying enzymes. *BMC Plant Biology*, *13*(1). https://doi.org/10.1186/1471-2229-13-24

Delaunois, B., Jeandet, P., Clément, C., Baillieul, F., Dorey, S., & Cordelier, S. (2014). Uncovering plant-pathogen crosstalk through apoplastic proteomic studies. *Frontiers in Plant Science*, *5*(249). https://doi.org/10.3389/fpls.2014.00249

Delauré, S. L., Van Hemelrijck, W., De Bolle, M. F. C., Cammue, B. P. A., & De Coninck, B. M. A. (2008). Building up plant defenses by breaking down proteins. *Plant Science*, *174*(4), 375–385. https://doi.org/10.1016/j.plantsci.2008.01.008

Díaz-Mendoza, M., Velasco-Arroyo, B., González-Melendi, P., Martínez, M., & Díaz, I. (2014). C1A cysteine protease–cystatin interactions in leaf senescence. *Journal of Experimental Botany*, *65*(14), 3825–3833. https://doi.org/10.1093/jxb/eru043

Ding, Y., Sun, T., Ao, K., Peng, Y., Zhang, Y., Li, X., & Zhang, Y. (2018). Opposite Roles of Salicylic Acid Receptors NPR1 and NPR3/NPR4 in Transcriptional Regulation of Plant Immunity. *Cell*, *173*(6), 1454-1467.e15. https://doi.org/10.1016/j.cell.2018.03.044

Domashevskiy, A. V., Miyoshi, H., & Goss, D. J. (2012). Inhibition of Pokeweed Antiviral Protein (PAP) by Turnip Mosaic Virus Genome-linked Protein (VPg). *Journal of Biological Chemistry*, *287*(35), 29729–29738. https://doi.org/10.1074/jbc.m112.367581

Duggar, B. M., & Armstrong, J. K. (1925). The Effect of Treating the Virus of Tobacco Mosaic With the Juices of Various Plants. *Annals of the Missouri Botanical Garden*, *12*(4), 359. https://doi.org/10.2307/2394061

Endo, Y., & Tsurugi, K. (1988). The RNA N-glycosidase activity of ricin A-chain. The characteristics of the enzymatic activity of ricin A-chain with ribosomes and with rRNA.

Journal of Biological Chemistry, *263*(18), 8735–8739. https://doi.org/10.1016/s0021-9258(18)68367-x

Evans, R., O'Neill, M., Pritzel, A., Antropova, N., Senior, A., Green, T., Žídek, A., Bates, R., Blackwell, S., Yim, J., Ronneberger, O., Bodenstein, S., Zielinski, M., Bridgland, A., Potapenko, A., Cowie, A., Tunyasuvunakool, K., Jain, R., Clancy, E., & Kohli, P. (2021). Protein complex prediction with AlphaFold-Multimer. *BioRxiv*. https://doi.org/10.1101/2021.10.04.463034

Fabbrini, M., Katayama, M., Nakase, I., & Vago, R. (2017). Plant Ribosome-Inactivating Proteins: Progesses, Challenges and Biotechnological Applications (and a Few Digressions). *Toxins*, *9*(10), 314. https://doi.org/10.3390/toxins9100314

Farvardin, A., González-Hernández, A. I., Llorens, E., García-Agustín, P., Scalschi, L., & Vicedo, B. (2020). The Apoplast: A Key Player in Plant Survival. *Antioxidants*, *9*(7), 604. https://doi.org/10.3390/antiox9070604

Felle, H. H. (2001). pH: Signal and Messenger in Plant Cells. *Plant Biology*, 3(6), 577–591. https://doi.org/10.1055/s-2001-19372

Felle, H. H., Herrmann, A., Hanstein, S., Hückelhoven, R., & Kogel, K.-H. (2004). Apoplastic pH Signaling in Barley Leaves Attacked by the Powdery Mildew Fungus Blumeria graminis f. sp. hordei. *Molecular Plant-Microbe Interactions®*, 17(1), 118–123. https://doi.org/10.1094/mpmi.2004.17.1.118

Felle, H. H., Waller, F., Molitor, A., & Kogel, K.-H. (2009). The Mycorrhiza Fungus Piriformospora indica Induces Fast Root-Surface pH Signaling and Primes Systemic Alkalinization of the Leaf Apoplast Upon Powdery Mildew Infection. *Molecular Plant-Microbe Interactions®*, 22(9), 1179–1185. https://doi.org/10.1094/mpmi-22-9-1179

Fernández-Fernández, Á. D., Stael, S., & Van Breusegem, F. (2023). Mechanisms controlling plant proteases and their substrates. *Cell Death & Differentiation*, *30*(4), 1047–1058. https://doi.org/10.1038/s41418-023-01120-5

Gandhi, R., Manzoor, M., & Hudak, K. A. (2008). Depurination of Brome Mosaic Virus RNA3 in Vivo Results in Translation-dependent Accelerated Degradation of the Viral RNA. *Journal of Biological Chemistry*, *283*(47), 32218–32228. https://doi.org/10.1074/jbc.m803785200

Geilfus, C.-M. (2017). The pH of the Apoplast: Dynamic Factor with Functional Impact Under Stress. *Molecular Plant*, *10*(11), 1371–1386. https://doi.org/10.1016/j.molp.2017.09.018

Geilfus, C.-M., Wang, L., Wu, J., & Xue, C. (2020). The pH of the leaf apoplast is critical for the formation of Pseudomonas syringae-induced lesions on leaves of the common bean (Phaseolus vulgaris). *Plant Science*, *290*(110328). https://doi.org/10.1016/j.plantsci.2019.110328

Geilfus, C.-M., Zhang, X., Mithöfer, A., Burgel, L., Bárdos, G., & Zörb, C. (2020). Leaf apoplastic alkalization promotes transcription of the ABA-synthesizing enzyme Vp14 and stomatal closure in *Zea mays*. *Journal of Experimental Botany*, *72*(7), 2686–2695. https://doi.org/10.1093/jxb/eraa589

Glazebrook, J. (2005). Contrasting Mechanisms of Defense Against Biotrophic and Necrotrophic Pathogens. *Annual Review of Phytopathology*, *43*(1), 205–227. https://doi.org/10.1146/annurev.phyto.43.040204.135923

Godson, A., & van der Hoorn, R. A. L. (2021). The front line of defence: a meta-analysis of apoplastic proteases in plant immunity. *Journal of Experimental Botany*, *72*(9), 3381–3394. https://doi.org/10.1093/jxb/eraa602

Gupta, R., Lee, S. E., Agrawal, G. K., Rakwal, R., Park, S., Wang, Y., & Kim, S. T. (2015). Understanding the plant-pathogen interactions in the context of proteomics-generated apoplastic proteins inventory. *Frontiers in Plant Science*, *6*(352). https://doi.org/10.3389/fpls.2015.00352

He, Y.-W., Guo, C.-X., Pan, Y.-F., Peng, C., & Weng, Z.-H. (2008). Inhibition of hepatitis B virus replication by pokeweed antiviral protein in vitro. *World Journal of Gastroenterology*, *14*(10), 1592. https://doi.org/10.3748/wjg.14.1592

Hou, S., Liu, Z., Shen, H., & Wu, D. (2019). Damage-Associated Molecular Pattern-Triggered Immunity in Plants. *Frontiers in Plant Science*, *10*(646). https://doi.org/10.3389/fpls.2019.00646

Hudak, K. A., Bauman, J. D., & Tumer, N. E. (2002). Pokeweed antiviral protein binds to the cap structure of eukaryotic mRNA and depurinates the mRNA downstream of the cap. *RNA*, *8*(9), 1148–1159. https://doi.org/10.1017/s1355838202026638

Hudak, K. A., Dinman, J. D., & Tumer, N. E. (1999). Pokeweed Antiviral Protein Accesses Ribosomes by Binding to L3. *Journal of Biological Chemistry*, *274*(6), 3859–3864. https://doi.org/10.1074/jbc.274.6.3859

Hudak, K. A., Parikh, B. A., Di, R., Baricevic, M., Santana, M., Seskar, M., & Tumer, N. E. (2004). Generation of pokeweed antiviral protein mutations in Saccharomyces cerevisiae: evidence that ribosome depurination is not sufficient for cytotoxicity. *Nucleic Acids Research*, *32*(14), 4244–4256. https://doi.org/10.1093/nar/gkh757

Hudak, K. A., Wang, P., & Tumer, N. E. (2000). A novel mechanism for inhibition of translation by pokeweed antiviral protein: Depurination of the capped RNA template. *RNA*, *6*(3), 369–380. https://doi.org/10.1017/s1355838200991337

Hur, Y., Hwang, D.-J., Zoubenko, O., Coetzer, C., Uckun, F. M., & Tumer, N. E. (1995). Isolation and characterization of pokeweed antiviral protein mutations in Saccharomyces cerevisiae: identification of residues important for toxicity. *Proceedings of the National Academy of Sciences of the United States of America*, 92(18), 8448–8452. https://doi.org/10.1073/pnas.92.18.8448

Iglesias, R., Pérez, Y., Carlos de Torre-Minguela, Ferreras, J. M., AntolínP., Jiménez, P., Ma, R., Méndez, E., & Tomás Girbés. (2005). Molecular characterization and systemic induction of single-chain ribosome-inactivating proteins (RIPs) in sugar beet (Beta vulgaris) leaves. *Journal of Experimental Botany*, *56*(416), 1675–1684. https://doi.org/10.1093/jxb/eri164

Irvin, J. D. (1975). Purification and partial characterization of the antiviral protein from Phytolacca americana which inhibits eukaryotic protein synthesis. *Archives of Biochemistry and Biophysics*, *169*(2), 522–528. https://doi.org/10.1016/0003-9861(75)90195-2

Irvin, J. D. (1983). Pokeweed antiviral protein. *Pharmacology & Therapeutics*, *21*(3), 371–387. https://doi.org/10.1016/0163-7258(83)90061-x

Jashni, M. K., Mehrabi, R., Collemare, J., Mesarich, C. H., & de Wit, P. J. G. M. (2015). The battle in the apoplast: further insights into the roles of proteases and their inhibitors in plant–pathogen interactions. *Frontiers in Plant Science*, *6*(584). https://doi.org/10.3389/fpls.2015.00584

Jelenska, J., Davern, S. M., Standaert, R. F., Mirzadeh, S., & Greenberg, J. T. (2017). Flagellin peptide flg22 gains access to long-distance trafficking in Arabidopsis via its receptor, FLS2. *Journal of Experimental Botany*, *68*(7), 1769–1783. https://doi.org/10.1093/jxb/erx060

Jiang, S., Pan, L., Zhou, Q., Xu, W., He, F., Zhang, L., & Gao, H. (2023). Analysis of the apoplast fluid proteome during the induction of systemic acquired resistance in *Arabidopsis thaliana*. *PeerJ*, *11*(e16324), e16324–e16324. https://doi.org/10.7717/peerj.16324

Jones, J. D. G., & Dangl, J. L. (2006). The plant immune system. *Nature*, *444*(7117), 323–329. https://doi.org/10.1038/nature05286

Jones, P., Binns, D., Chang, H.-Y., Fraser, M., Li, W., McAnulla, C., McWilliam, H., Maslen, J., Mitchell, A., Nuka, G., Pesseat, S., Quinn, A. F., Sangrador-Vegas, A., Scheremetjew, M., Yong, S.-Y., Lopez, R., & Hunter, S. (2014). InterProScan 5: genome-scale protein function classification. *Bioinformatics*, *30*(9), 1236–1240. https://doi.org/10.1093/bioinformatics/btu031

Jumper, J., Evans, R., Pritzel, A., Green, T., Figurnov, M., Ronneberger, O., Tunyasuvunakool, K., Bates, R., Žídek, A., Potapenko, A., Bridgland, A., Meyer, C., Kohl, S. A. A., Ballard, A. J., Cowie, A., Romera-Paredes, B., Nikolov, S., Jain, R., Adler, J., & Back, T. (2021). Highly accurate protein structure prediction with AlphaFold. *Nature*, *596*(7873), 583–589. https://www.nature.com/articles/s41586-021-03819-2

Karimi, H. Z., Baldrich, P., Rutter, B. D., Borniego, L., Zajt, K. K., Meyers, B. C., & Innes, R. W. (2022). Arabidopsis apoplastic fluid contains sRNA- and circular RNA-protein complexes that are located outside extracellular vesicles. *The Plant Cell*, *34*(5), koac043. https://doi.org/10.1093/plcell/koac043

Karran, R. A., & Hudak, K. A. (2008). Depurination within the intergenic region of Brome mosaic virus RNA3 inhibits viral replication in vitro and in vivo. *Nucleic Acids Research*, *36*(22), 7230–7239. https://doi.org/10.1093/nar/gkn896

Koo, Y. M., Heo, A. Y., & Choi, H. W. (2020). Salicylic Acid as a Safe Plant Protector and Growth Regulator. *The Plant Pathology Journal*, *36*(1), 1–10. https://doi.org/10.5423/PPJ.RW.12.2019.0295

Krivdova, G., & Hudak, K. A. (2015). Pokeweed antiviral protein restores levels of cellular APOBEC3G during HIV-1 infection by depurinating Vif mRNA. *Antiviral Research*, *122*, 51–54. https://doi.org/10.1016/j.antiviral.2015.08.007

Kruger, J. (2002). A Tomato Cysteine Protease Required for Cf-2-Dependent Disease Resistance and Suppression of Autonecrosis. *Science*, *296*(5568), 744–747. https://doi.org/10.1126/science.1069288

Kumar, R., Bhattacharjee, A., & Tiwari, S. (2021). Plant-derived ribosome-inactivating proteins involved in defense against plant viruses. *European Journal of Plant Pathology*, *162*(3), 515–537. https://doi.org/10.1007/s10658-021-02426-1

Liu, H., Hu, M., Wang, Q., Cheng, L., & Zhang, Z. (2018). Role of Papain-Like Cysteine Proteases in Plant Development. *Frontiers in Plant Science*, *9*(1717). https://doi.org/10.3389/fpls.2018.01717

Liu, P., Shi, C., Liu, S., Lei, J., Lu, Q., Hu, H., Ren, Y., Zhang, N., Sun, C., Chen, L., Jiang, Y., Feng, L., Zhang, T., Zhong, K., Liu, J., Zhang, J., Zhang, Z., Sun, B., Chen, J., & Tang, Y. (2023). A papain-like cysteine protease-released small signal peptide confers wheat resistance to wheat yellow mosaic virus. *Nature Communications*, *14*(1). https://doi.org/10.1038/s41467-023-43643-y

Lodge, J. K., Kaniewski, W. K., & Tumer, N. E. (1993). Broad-spectrum virus resistance in transgenic plants expressing pokeweed antiviral protein. *Proceedings of the National Academy of Sciences*, *90*(15), 7089–7093. https://doi.org/10.1073/pnas.90.15.7089

Macho, A. P., & Zipfel, C. (2014). Plant PRRs and the activation of innate immune signaling. *Molecular Cell*, *54*(2), 263–272. https://doi.org/10.1016/j.molcel.2014.03.028
Manguy, J., Jehl, P., Dillon, E., Davey, N. E., Shields, D. C., & Holton, T. A. (2016). Peptigram: A Web-Based Application for Peptidomics Data Visualization. *Journal of Proteome Research*, *16*(2), 712–719. https://doi.org/10.1021/acs.jproteome.6b00751
Mansouri, S., Choudhary, G., Sarzala, P. M., Ratner, L., & Hudak, K. A. (2009). Suppression of Human T-cell Leukemia Virus I Gene Expression by Pokeweed Antiviral Protein. *Journal of Biological Chemistry*, *284*(45), 31453–31462. https://doi.org/10.1074/jbc.m109.046235
Marchant, A., & Hartley, M. R. (1995). The Action of Pokeweed Antiviral Protein and Ricin A-chain on Mutants in the α-Sarcin Loop ofEscherichia coli23S Ribosomal RNA. *Journal of Molecular Biology*, *254*(5), 848–855. https://doi.org/10.1006/jmbi.1995.0660
Martinez, M., Cambra, I., Carrillo, L., Diaz-Mendoza, M., & Diaz, I. (2009). Characterization of the Entire Cystatin Gene Family in Barley and Their Target Cathepsin L-Like Cysteine-Proteases, Partners in the Hordein Mobilization during Seed Germination . *Plant Physiology*, *151*(3), 1531–1545. https://doi.org/10.1104/pp.109.146019
Martínez, M., Cambra, I., González-Melendi, P., Santamaría, M. E., & Díaz, I. (2012). C1A cysteine-proteases and their inhibitors in plants. *Physiologia Plantarum*, *145*(1), 85–94. https://doi.org/10.1111/j.1399-3054.2012.01569.x
Meena, M., Yadav, G., Sonigra, P., Nagda, A., Mehta, T., Swapnil, P., Harish, & Marwal, A. (2022). Role of elicitors to initiate the induction of systemic resistance in plants to biotic stress. *Plant Stress*, *5*(100103), 100103. https://doi.org/10.1016/j.stress.2022.100103
Miedes, E., Vanholme, R., Boerjan, W., & Molina, A. (2014). The role of the secondary cell wall in plant resistance to pathogens. *Frontiers in Plant Science*, *5*(358). https://doi.org/10.3389/fpls.2014.00358
Mirdita, M., Schütze, K., Moriwaki, Y., Heo, L., Ovchinnikov, S., & Steinegger, M. (2022). ColabFold: making protein folding accessible to all. *Nature Methods*, *19*(6), 1–4. https://doi.org/10.1038/s41592-022-01488-1
Misas-Villamil, J. C., van der Hoorn, R. A. L., & Doehlemann, G. (2016). Papain-like cysteine proteases as hubs in plant immunity. *New Phytologist*, *212*(4), 902–907. https://doi.org/10.1111/nph.14117
Montanaro, L., Sperti, S., Mattioli, A., Testoni, G., & Stirpe, F. (1975). Inhibition by ricin of protein synthesisin vitro. Inhibition of the binding of elongation factor 2 and of adenosine diphosphate-ribosylated elongation factor 2 to ribosomes. *Biochemical Journal*, *146*(1), 127–131. https://doi.org/10.1042/bj1460127
Monzingo, A. F., Collins, E. J., Ernst, S. R., Irvin, J. D., & Robertus, J. D. (1993). The 2·5 Å Structure of Pokeweed Antiviral Protein. *Journal of Molecular Biology*, *233*(4), 705–715. https://doi.org/10.1006/jmbi.1993.1547
Mott, G. A., Middleton, M. A., Desveaux, D., & Guttman, D. S. (2014). Peptides and small molecules of the plant-pathogen apoplastic arena. *Frontiers in Plant Science*, *5*(677). https://doi.org/10.3389/fpls.2014.00677
Mueller, A. N., Ziemann, S., Treitschke, S., Aßmann, D., & Doehlemann, G. (2013). Compatibility in the Ustilago maydis–Maize Interaction Requires Inhibition of Host Cysteine Proteases by the Fungal Effector Pit2. *PLoS Pathogens*, *9*(2), e1003177. https://doi.org/10.1371/journal.ppat.1003177
Nakagawa, T., Suzuki, T., Murata, S., Nakamura, S., Hino, T., Maeo, K., Tabata, R., Kawai, T.,

Tanaka, K., Niwa, Y., Watanabe, Y., Nakamura, K., Kimura, T., & Ishiguro, S. (2007). Improved Gateway binary vectors: high-performance vectors for creation of fusion constructs in transgenic analysis of plants. *Bioscience, Biotechnology, and Biochemistry*, *71*(8), 2095–2100. https://doi.org/10.1271/bbb.70216

Neller, K. C. M., Diaz, C. A., Platts, A. E., & Hudak, K. A. (2019). De novo Assembly of the Pokeweed Genome Provides Insight Into Pokeweed Antiviral Protein (PAP) Gene Expression. *Frontiers in Plant Science*, *10*(1002). https://doi.org/10.3389/fpls.2019.01002

Neller, K. C. M., Klenov, A., & Hudak, K. A. (2016). The Pokeweed Leaf mRNA Transcriptome and Its Regulation by Jasmonic Acid. *Frontiers in Plant Science*, *7*(283). https://doi.org/10.3389/fpls.2016.00283

O'Leary, B. M., Rico, A., McCraw, S., Fones, H. N., & Preston, G. M. (2014). The Infiltration-centrifugation Technique for Extraction of Apoplastic Fluid from Plant Leaves Using Phaseolus vulgaris as an Example. *Journal of Visualized Experiments*, *94*. https://doi.org/10.3791/52113

Osborn, R. W., & Hartley, M. R. (1990). Dual effects of the ricin A chain on protein synthesis in rabbit reticulocyte lysate. Inhibition of initiation and translocation. *European Journal of Biochemistry*, *193*(2), 401–407. https://doi.org/10.1111/j.1432-1033.1990.tb19353.x

Pengpeng Lü, Liu, Y., Yu, X., Shi, C.-L., & Liu, X. (2022). The right microbe-associated molecular patterns for effective recognition by plants. *Frontiers in Microbiology*, *13*(1019069). https://doi.org/10.3389/fmicb.2022.1019069

Pérez-López, E., Hossain, M. M., Wei, Y., Todd, C. D., & Bonham-Smith, P. C. (2021). A clubroot pathogen effector targets cruciferous cysteine proteases to suppress plant immunity. *Virulence*, *12*(1), 2327–2340. https://doi.org/10.1080/21505594.2021.1968684

Picard, D., Kao, C.-H., & Hudak, K. A. (2005). Pokeweed Antiviral Protein Inhibits Brome Mosaic Virus Replication in Plant Cells. *Journal of Biological Chemistry*, *280*(20), 20069–20075. https://doi.org/10.1074/jbc.m413452200

Planas-Marquès, M., Bernardo-Faura, M., Paulus, J. K., Farnusch Kaschani, Kaiser, M., Valls, M., van, & Coll, N. S. (2018). Protease Activities Triggered by Ralstonia solanacearum Infection in Susceptible and Tolerant Tomato Lines. *Molecular & Cellular Proteomics*, *17*(6), 1112–1125. https://doi.org/10.1074/mcp.ra117.000052

Prashar, T., De La Selle, F., & Hudak, K. A. (2023). Abasic RNA: its formation and potential role in cellular stress response. *RNA Biology*, *20*(1), 348–358. https://doi.org/10.1080/15476286.2023.2223466

Qin, X., Zheng, X., Shao, C., Gao, J., Jiang, L., Zhu, X., Yan, F., Tang, L., Xu, Y., & Chen, F. (2009). Stress-induced curcin-L promoter in leaves of Jatropha curcas L. and characterization in transgenic tobacco. *Planta*, *230*(2), 387–395. https://doi.org/10.1007/s00425-009-0956-9

Rajamohan, F., Igor Kurinov, Venkatachalam, T. K., & Uckun, F. M. (1999). Deguanylation of Human Immunodeficiency Virus (HIV-1) RNA by Recombinant Pokeweed Antiviral Protein. *Biochemical and Biophysical Research Communications*, *263*(2), 419–424. https://doi.org/10.1006/bbrc.1999.1335

Rajamohan, F., Venkatachalam, T. K., Irvin, J. D., & Uckun, F. M. (1999). Pokeweed Antiviral Protein Isoforms PAP-I, PAP-II, and PAP-III Depurinate RNA of Human Immunodeficiency Virus (HIV)-1. *Biochemical and Biophysical Research Communications*, *260*(2), 453–458. https://doi.org/10.1006/bbrc.1999.0922

Rawlings, N. D., & Bateman, A. (2020). How to use to use MEROPS database and website to help understand peptidase specificity. *Protein Science*, *30*(1), 83–92. https://doi.org/10.1002/pro.3948

Ready, M. P., Brown, D. T., & Robertus, J. D. (1986). Extracellular localization of pokeweed antiviral protein. *Proceedings of the National Academy of Sciences of the United States of America*, *83*(14), 5053–5056. https://doi.org/10.1073/pnas.83.14.5053

Shabab, M., Shindo, T., Gu, C., Kaschani, F., Pansuriya, T., Chintha, R., Harzen, A., Colby, T., Kamoun, S., & van der Hoorn, R. A. L. (2008). Fungal Effector Protein AVR2 Targets Diversifying Defense-Related Cys Proteases of Tomato. *The Plant Cell*, *20*(4), 1169–1183. https://doi.org/10.1105/tpc.107.056325

Shi, W.-W., Mak, A., Wong, K.-B., & Shaw, P.-C. (2016). Structures and Ribosomal Interaction of Ribosome-Inactivating Proteins. *Molecules*, *21*(11), 1588. https://doi.org/10.3390/molecules21111588

Song, S.-K., Choi, Y., Moon, Y. H., Kim, S.-G., Choi, Y. D., & Lee, J. S. (2000). Systemic induction of a Phytolacca insularis antiviral protein gene by mechanical wounding, jasmonic acid, and abscisic acid. *Plant Molecular Biology*, *43*(4), 439–450. https://doi.org/10.1023/a:1006444322626

Spoel, S. H., & Dong, X. (2024). Salicylic Acid in Plant Immunity and Beyond. *The Plant Cell*, *36*(5). https://doi.org/10.1093/plcell/koad329

Sun, Y., Li, L., Macho, A. P., Han, Z., Hu, Z., Zipfel, C., Zhou, J.-M. ., & Chai, J. (2013). Structural Basis for flg22-Induced Activation of the Arabidopsis FLS2-BAK1 Immune Complex. *Science*, *342*(6158), 624–628. https://doi.org/10.1126/science.1243825

Taiz, L., Zeiger, E., Møller, I. M., & Murphy, A. S. (2015). *Plant Physiology and Development* (6th ed.). Sinauer Associates, Inc., Publishers.

Tamaoki, D., Seo, S., Yamada, S., Kano, A., Miyamoto, A., Shishido, H., Miyoshi, S., Taniguchi, S., Akimitsu, K., & Gomi, K. (2013). Jasmonic acid and salicylic acid activate a common defense system in rice. *Plant Signaling & Behavior*, *8*(6). https://doi.org/10.4161/psb.24260

Taylor, S. C., Nadeau, K., Abbasi, M., Lachance, C., Nguyen, M., & Fenrich, J. (2019). The Ultimate qPCR Experiment: Producing Publication Quality, Reproducible Data the First Time. *Trends in Biotechnology*, *37*(7), 761–774. https://doi.org/10.1016/j.tibtech.2018.12.002

Teufel, F., Almagro Armenteros, J. J., Johansen, A. R., Gíslason, M. H., Pihl, S. I., Tsirigos, K. D., Winther, O., Brunak, S., von Heijne, G., & Nielsen, H. (2022). SignalP 6.0 predicts all five types of signal peptides using protein language models. *Nature Biotechnology*, *40*(7). https://doi.org/10.1038/s41587-021-01156-3

Thumuluri, V., Almagro Armenteros, J. J., Johansen, A., Nielsen, H., & Winther, O. (2022). DeepLoc 2.0: multi-label subcellular localization prediction using protein language models. *Nucleic Acids Research*, *50*(W1). https://doi.org/10.1093/nar/gkac278

Tomlinson, J. A., Walker, V. M., Flewett, T. H., & Barclay, G. R. (1974). The Inhibition of Infection by Cucumber Mosaic Virus and Influenza Virus by Extracts from Phytolacca americana. *Journal of General Virology*, *22*(2), 225–232. https://doi.org/10.1099/0022-1317-22-2-225

Turk, B., Turk, D., & Turk, V. (2012). Protease signalling: the cutting edge. *The EMBO Journal*, *31*(7), 1630–1643. https://doi.org/10.1038/emboj.2012.42

Uckun, F. M., Rajamohan, F., Pendergrass, S., Zahide Özer, Waurzyniak, B., & Chen, M.

(2003). Structure-Based Design and Engineering of a Nontoxic Recombinant Pokeweed Antiviral Protein with Potent Anti-Human Immunodeficiency Virus Activity. *Antimicrobial Agents and Chemotherapy*, *47*(3), 1052–1061. https://doi.org/10.1128/aac.47.3.1052-1061.2003

Ussery, M. A., Irvin, J. D., & Hardesty, B. (1977). INHIBITION OF POLIOVIRUS REPLICATION BY A PLANT ANTIVIRAL PEPTIDE. *Annals of the New York Academy of Sciences*, *284*(1 Third Confere), 431–440. https://doi.org/10.1111/j.1749-6632.1977.tb21979.x

van der Hoorn, R. A. L. (2008). Plant Proteases: From Phenotypes to Molecular Mechanisms. *Annual Review of Plant Biology*, *59*(1), 191–223. https://doi.org/10.1146/annurev.arplant.59.032607.092835

van der Hoorn, R. A. L., & Kamoun, S. (2008). From Guard to Decoy: A New Model for Perception of Plant Pathogen Effectors. *The Plant Cell*, *20*(8), 2009–2017. https://doi.org/10.1105/tpc.108.060194

van der Linde, K., Hemetsberger, C., Kastner, C., Kaschani, F., van der Hoorn, R. A. L., Kumlehn, J., & Doehlemann, G. (2012). A Maize Cystatin Suppresses Host Immunity by Inhibiting Apoplastic Cysteine Proteases. *The Plant Cell*, *24*(3), 1285–1300. https://doi.org/10.1105/tpc.111.093732

van der Linde, K., Mueller, A. N., Hemetsberger, C., Kashani, F., van der Hoorn, R. A. L., & Doehlemann, G. (2012). The maize cystatin CC9 interacts with apoplastic cysteine proteases. *Plant Signaling & Behavior*, *7*(11), 1397–1401. https://doi.org/10.4161/psb.21902

van Esse, H. P., van't Klooster, J. W., Bolton, M. D., Yadeta, K. A., van Baarlen, P., Boeren, S., Vervoort, J., de Wit, P. J. G. M., & Thomma, B. P. H. J. (2008). The *Cladosporium fulvum* Virulence Protein Avr2 Inhibits Host Proteases Required for Basal Defense . *The Plant Cell*, *20*(7), 1948–1963. https://doi.org/10.1105/tpc.108.059394

Váradi, M., Bertoni, D., Magaña, P., Paramval, U., Pidruchna, I., Radhakrishnan, M., Tsenkov, M., Nair, S., Mirdita, M., Yeo, J., Kovalevskiy, O., Tunyasuvunakool, K., Laydon, A., Žídek, A., Tomlinson, H., Hariharan, D., Abrahamson, J., Green, T., Jumper, J., & Birney, E. (2023). AlphaFold Protein Structure Database in 2024: providing structure coverage for over 214 million protein sequences. *Nucleic Acids Research*, *52*(D1). https://doi.org/10.1093/nar/gkad1011

Verma, V., Ravindran, P., & Kumar, P. P. (2016). Plant hormone-mediated regulation of stress responses. *BMC Plant Biology*, *16*(1). https://doi.org/10.1186/s12870-016-0771-y

Vivanco, J. M., & Tumer, N. E. (2003). Translation Inhibition of Capped and Uncapped Viral RNAs Mediated by Ribosome-Inactivating Proteins. *Phytopathology®*, *93*(5), 588–595. https://doi.org/10.1094/phyto.2003.93.5.588

Wang, M., & Hudak, K. A. (2006). A novel interaction of pokeweed antiviral protein with translation initiation factors 4G and iso4G: a potential indirect mechanism to access viral RNAs. *Nucleic Acids Research*, *34*(4), 1174–1181. https://doi.org/10.1093/nar/gkj520

Wang, Y., Mostafa, S., Zeng, W., & Jin, B. (2021). Function and Mechanism of Jasmonic Acid in Plant Responses to Abiotic and Biotic Stresses. *International Journal of Molecular Sciences*, *22*(16), 8568. https://doi.org/10.3390/ijms22168568

Wang, Y., Wang, Y., & Wang, Y. (2020). Apoplastic Proteases: Powerful Weapons against Pathogen Infection in Plants. *Plant Communications*, *1*(4), 100085. https://doi.org/10.1016/j.xplc.2020.100085

Yamada, K., Matsushima, R., Nishimura, M., & Hara-Nishimura, I. (2001). A Slow Maturation of a Cysteine Protease with a Granulin Domain in the Vacuoles of Senescing Arabidopsis Leaves. *Plant Physiology*, *127*(4), 1626–1634. https://doi.org/10.1104/pp.010551

Yamaguchi, K., & Kawasaki, T. (2021). Pathogen- and plant-derived peptides trigger plant immunity. *Peptides*, *144*(170611), 170611. https://doi.org/10.1016/j.peptides.2021.170611

Yang, Y.-X., Ahammed, G., Wu, C., Fan, S., & Zhou, Y.-H. (2015). Crosstalk among Jasmonate, Salicylate and Ethylene Signaling Pathways in Plant Disease and Immune Responses. *Current Protein & Peptide Science*, *16*(5), 450–461. https://doi.org/10.2174/1389203716666150330141638

Yuan, W., Chen, X., Du, K., Jiang, T., Li, M., Cao, Y., Li, X., Doehlemann, G., Fan, Z., & Zhou, T. (2024). NIa-Pro of sugarcane mosaic virus targets Corn Cysteine Protease 1 (CCP1) to undermine salicylic acid-mediated defense in maize. *PLOS Pathogens*, *20*(3), e1012086–e1012086. https://doi.org/10.1371/journal.ppat.1012086

Zeng, Z.-H., He, X.-L., Li, H.-M., Hu, Z., & Wang, D.-C. (2003). Crystal structure of pokeweed antiviral protein with well-defined sugars from seeds at 1.8Å resolution. *Journal of Structural Biology*, *141*(2), 171–178. https://doi.org/10.1016/s1047-8477(02)00580-4

Zhang, B., Tremousaygue, D., Denancé, N., Peter, Hörger, A. C., Dabos, P., Goffner, D., Thomma, B. P. H. J., van, & Tuominen, H. (2014). PIRIN2 stabilizes cysteine proteaseXCP2 and increases susceptibility to the vascular pathogen*Ralstonia solanacearum*in Arabidopsis. *Plant Journal*, *79*(6), 1009–1019. https://doi.org/10.1111/tpj.12602

Zhou, J.-M., & Zhang, Y. (2020). Plant Immunity: Danger Perception and Signaling. *Cell*, *181*(5), 978–989. https://doi.org/10.1016/j.cell.2020.04.028

Zhu, F., Zhou, Y.-K., Ji, Z.-L., & Chen, X.-R. (2018). The Plant Ribosome-Inactivating Proteins Play Important Roles in Defense against Pathogens and Insect Pest Attacks. *Frontiers in Plant Science*, *9*(146). https://doi.org/10.3389/fpls.2018.00146

Ziemann, S., van der Linde, K., Lahrmann, U., Acar, B., Kaschani, F., Colby, T., Kaiser, M., Ding, Y., Schmelz, E., Huffaker, A., Holton, N., Zipfel, C., & Doehlemann, G. (2018). An apoplastic peptide activates salicylic acid signalling in maize. *Nature Plants*, *4*(3), 172–180. https://doi.org/10.1038/s41477-018-0116-y

APPENDIX A: SUPPLEMENTAL FIGURE

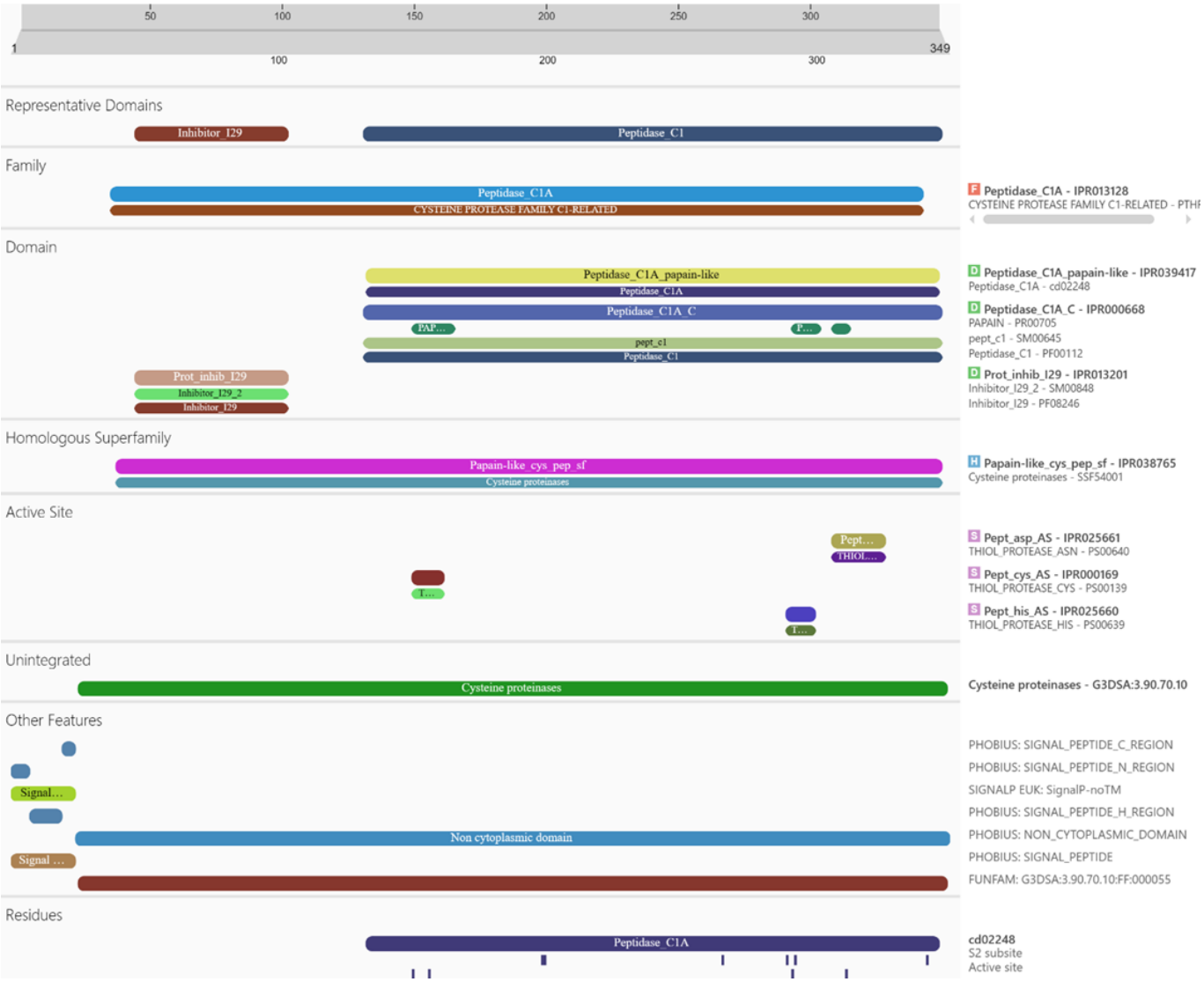

Supplemental Figure 1. InterproScan search results for PaCP1 amino acid sequence. Screenshot of the InterproScan results using the PaCP1 amino acid sequence as the input. Information from the InterPro database was used to identify protein domains, superfamily, active sites, and other features. Identified features are represented by colored bars to indicate which amino acids they span, with corresponding Interproscan description and identifier on the right-hand side.

APPENDIX B: LIST OF PRIMERS

Table 2: List of primers used for various methods

Name	Sequence	What it was used for
PAP-I-35-For	ATAACTGCATGTTCTCATAAAAAAGCCTCAGC	PAP qPCR
PAP-I-112-83 Rev	CTTCCTACTAGCTAGTTCCAATACTTTCGC	PAP qPCR
PAP-I- RT-Rev23	GTTTATGATCAGAATCCTTCAAATAGATCACCAAG	PAP qPCR RT
attB1 adapter	GGGGACAAGTTTGTACAAAAAAGCAGGCT	Generation of full attB PCR products
attB2 adapter	GGGGACCACTTTGTACAAGAAAGCTGGGT	Generation of full attB PCR products
attB1 For PAP-1	AAAAAGCAGGCTGTGAATACAATCATCTACAATGT TGGAAGTACCAC	Generation of mature PAP clone for Y2H
attB2 Rev PAP-1	AGAAAGCTGGGTTCATCAATAAGTTGTCTGACAGC	Generation of mature PAP clone for Y2H
attB1 For Pro-PaCP1	AAAAAGCAGGCTCTCGTGACTTCTCAATCGTCGGT TATTC	Generation of Pro-PaCP1 clone for Y2H
attB1 For mPaCP1	AAAAAGCAGGCTCTAAGTCTGTAGACTGGAGAAA GA	Generation of mature PaCP1 clone for Y2H
attB2 Rev PaCP1	AGAAAGCTGGGTTCATCATCATTTCTTCTTGATAGG	Generation of mature PaCP1 and Pro-PaCP1 clone for Y2H
attB1 For Full PaCP1	AAAAAGCAGGCTCTATGGCTCTTTCCCTATACAACT T	Generation of PaCP1 agroinfiltration clone
attB2 Rev Full PaCP1	AGAAAGCTGGGTTTTTCTTCTTGATAGGGTAAGA	Generation of PaCP1 agroinfiltration clone
PaCP1 For 1	GACACCGAGATGTTCCAGAGAATG	PaCP1 qPCR
PaCP1 Rev 1	AAACTGAAAGTCCCTCCCAGATG	PaCP1 qPCR
PaCP1 RT Rev	GCTTGGTGTTCCTCTTCATTC	PaCP1 qPCR RT
PR1 For 2	GGAGAGAACATTGCATGGAGTAGC	PR1 qPCR
PR1 Rev 2	CAGGAGCACACGTGTTGGAATTA	PR1 qPCR and RT
25S rRNA reference	AGACCGTCGCTTGCTACAAT	Positive control Figure 9C

25S rRNA reference	ATGACGAGGCATTTGGCTAC	Positive control Figure 9C
23978 For	GGGAGCAACCTTTGGGATTAC	Internal control gene for qPCR
23978 Rev	CATAGAGCAAGCTGCGGTTAG	Internal control gene for qPCR
23978 RT	TCAGAAACTTGCATCTTCAGTTGTGGGCCGT	Internal control gene for qPCR
17908 For	GTTGGTAAAGCCCAGAAGAAGG	Internal control gene for qPCR
17908 Rev	GTAGAGGTTTGTGCCTTGGTATTT	Internal control gene for qPCR
17908 RT	GGGAGCAACCTTTGGGATTAC	Internal control gene for qPCR